LLNL-JRNL-872960

A buoyancy–shear–drag–scalar-based turbulence model for power-law acceleration-driven Rayleigh–Taylor, reshocked Richtmyer–Meshkov, and Kelvin–Helmholtz mixing

Oleg Schilling

Lawrence Livermore National Laboratory, P.O. Box 808, Livermore, CA 94550, USA

Abstract

A previously developed phenomenological turbulence model for Rayleigh–Taylor, reshocked Richtmyer–Meshkov, and Kelvin–Helmholtz instability-induced mixing based on a general buoyancy–shear–drag model [O. Schilling, "A buoyancy–shear–drag-based turbulence model for Rayleigh–Taylor, reshocked Richtmyer–Meshkov, and Kelvin–Helmholtz mixing," Physica D **402**, 132238 (2020)] is extended to include active or passive scalar mixing and power-law acceleration-driven Rayleigh–Taylor mixing. The buoyancy–shear–drag equations are coupled to a scalar variance equation that is used to define the molecular mixing parameter θ_m, and when the scalar is active, modifies the Rayleigh–Taylor and Kelvin–Helmholtz mixing layer growth parameters to depend on the asymptotic value of this parameter, θ_{mol}. The scalar variance equation is closed by algebraically or differentially modeling the scalar variance dissipation rate. Nonlinear analytical solutions of the model are obtained in the total and separate bubble and spike mixing layer width formulations with the algebraic scalar variance dissipation rate for each instability, which are then used to calibrate the mechanical and scalar equation coefficients to predict specific values of physical observables and molecular mixing parameters. Surrogate mechanical and scalar turbulent fields can be constructed by multiplying a presumed self-similar spatial profile by appropriate functions of the width and its time derivative, and of the scalar obtained by solving the ordinary differential model equations. *The explicit modeling and solution of turbulent transport equations are not required.* The bubble and spike mixing layer width and scalar variance equations are then solved numerically for constant-acceleration Rayleigh–Taylor, impulsively reshocked Richtmyer–Meshkov, and Kelvin–Helmholtz mixing, confirming that the prescribed level of molecular mixing is correctly predicted and illustrating the spatiotemporal evolution of the scalar fields.

Keywords: Turbulent mixing, Scalar mixing, Rayleigh–Taylor, Richtmyer–Meshkov, Kelvin–Helmholtz, Buoyancy–drag

1. Introduction

Turbulent mixing of single- and multiple-species fluids is encountered in nature (e.g., geophysical flows in the atmosphere and oceans, and astrophysical flows) and a variety of technological applications (e.g., combustion, chemical and process engineering, and inertial fusion). In many of the flows involving multiple fluids, the species are initially separated by a perturbed diffuse or sharp interface and subject to density, pressure, velocity, and concentration gradients induced, for example, by continuous or discontinuous accelerations and shear. Mixing processes that may lead to the development of nonlinear, transitional, and perhaps turbulent flows are therefore described by both mechanical and scalar fields. Here, mechanical fields refer to quantities derived from velocity fields, such as the kinetic energy and its dissipation rate, while scalar fields refer to quantities such as mass fraction, density, or concentration. For the class of multifluid flows that are Rayleigh–Taylor, Richtmyer–Meshkov, or Kelvin–Helmholtz unstable (see Ref. [1] for a survey), the *extent* of the mixing layer is described by mechanical fields while the *intensity* of mixing within the layer is described by scalar fields such as a scalar variance. In particular, the amount of *molecular mixing* between two species is typically characterized by a molecular mixing parameter related to the magnitude of scalar fluctuations during the entrainment, stirring, and diffusive mixing stages [2].

Within the context of Reynolds-averaged turbulence models, the BHRZ model [3] was an early model that used a transport equation for the averaged Favre fluctuating velocity $\widetilde{v_i''}$ (the negative of the turbulent mass flux a_i) rather than an algebraic closure, which contained a buoyancy production term $b\partial\overline{p}/\partial x_i$ with $b = -\overline{\rho'(1/\rho)'}$ the negative density–specific volume correlation depending on (scalar) density fluctuations. A second-order model was later developed for Richtmyer–Meshkov mixing that included a transport equation for the density variance [4]. The much more recent K–L–a–V model [5] expresses b algebraically in terms of the mass fraction variance V for the binary mixing case [6].

Email address: schilling1@llnl.gov (Oleg Schilling)

As discussed and motivated in Ref. [7], in the modeling of complex applications involving hydrodynamic instabilities, it is still too computationally expensive to use direct and large-eddy simulation routinely. Therefore, reduced order modeling approaches such as Reynolds-averaged modeling continue to be used extensively in multiphysics codes. In such approaches, mean field transport equations coupled to turbulent transport equations are solved, which are partial differential equations in space and time. Analytical self-similar solutions of these equations obtained in particular limiting cases provide insight into the physics of the turbulent hydrodynamic instability production, dissipation, and diffusion mechanisms, and provide a systematic approach for the analytical calibration of the model coefficients in the small Atwood number limit [7–9]. However, it also useful to develop even simpler reduced order models based on the buoyancy–drag paradigm that can predict mean and turbulent fields that are similar to those obtained from Reynolds-averaged models as developed, described, and applied in Ref. [10].

Buoyancy–drag models are a class of simple ordinary differential models that have been used to evolve bubble, spike, and total mixing layer widths arising from Rayleigh–Taylor, Richtmyer–Meshkov, and Kelvin–Helmholtz instabilities in time, as summarized in Ref. [10]. These models have been applied in the linear, nonlinear, and turbulent regimes, and provide an intuitively appealing representation of the basic large-scale dynamics of these complex instabilities and the mechanical mixing arising from them. In the turbulent regime, the models give widths that are consistent with generally accepted self-similar scalings. For example, early time modifications to the standard buoyancy–drag model for Richtmyer–Meshkov mixing were proposed [11] based on analysis of implicit large-eddy simulation (ILES) data from the `FLAMENCO` code corresponding to the Mach 1.84 and Atwood number 0.5 multimode instability with narrowband initial conditions considered previously [12]. This modified buoyancy–drag model was subsequently generalized to separate equations for the bubble and spike widths [13]. Buoyancy–drag modeling of bubble and spike distances in three-dimensional spherical implosions was also explored numerically using the `FLAMENCO` code [14].

The present work extends the buoyancy–shear–drag turbulence model formulated in Ref. [10] to include scalar fluctuations. Conceptually, the

model is motivated by the observation that Reynolds-averaged turbulence models based on a description of mechanical and scalar turbulent mixing in one spatial dimension aligned with the direction of transport have self-similar solutions in the infinite Reynolds number limit, in which the spatiotemporal dependence of the turbulent fields $\{\phi\}$ decouple into products of temporal power-laws $A_\phi t^{\theta_\phi}$ (where the prefactors $\{A_\phi\}$ are functions of the model coefficients and physical parameters) and self-similar spatial profiles $f_\phi(z/h(t))$ [where z is the direction of transport and $h(t)$ is the mixing layer width] [7]. When those equations are integrated over z, the inhomogeneous turbulent diffusion terms vanish because the flux terms vanish at the boundaries of the mixing layer and the resulting equations depend only on time: this 'zero-dimensional' approximation was extensively analyzed by Llor [15, 16] in the context of single-fluid K–ϵ and two-fluid models applied to the instabilities considered here. The present buoyancy–shear–drag–scalar (BSDS) model can be similarly interpreted as a zero-dimensional model in which the amplitudes of the time-dependent turbulent fields are determined by the solutions of the ordinary differential equations subject to some chosen initial conditions.

The further phenomenological extension of the model to describe one-dimensional turbulent fields by multiplying the time-dependent fields by assumed self-similar spatial profiles is analogous to the self-similar approximation made in the analysis of Reynolds-averaged models. The resulting one-dimensional fields grow in amplitude according to the temporal solutions and widen in space according to the growth of the mixing layer width. The constant prefactors multiplying the fields depend on the BSDS model coefficients and physical parameters of the instabilities (e.g., acceleration, Atwood number).

The details of the approximations and general model formulation, and how they were used to generate mean and turbulent fields are not repeated here. Briefly, instead of solving turbulent transport equations to obtain a turbulent diffusivity and viscosity for gradient-diffusion closures, the turbulent diffusivity and viscosity are constructed as spatial profiles by:

1. solving the BSDS equations for the bubble and spike mixing layer widths h_b and h_s or for the total width $h = h_b + h_s$ and the scalar variance and its dissipation rate;
2. using the bubble and spike widths or the total width and their rates of change dh_b/dt and dh_s/dt or dh/dt to obtain a time-dependent turbulent diffusivity and viscosity $D_t, \nu_t \propto hdh/dt$, and;
3. constructing a space–time turbulent diffusivity (or viscosity) by multiplying the time-dependent value by a profile of the form $f(z/h_b, z/h_s)$ or a self-similar profile of the form $f(z/h)$ in the total width formulation, where $\eta \propto z/h(t)$ is the similarity variable (z is the coordinate along the direction of acceleration or shock).

The resulting turbulent diffusivity $D_t(z,t)$ and viscosity $\nu_t(z,t)$ can then be used to construct the usual gradient-diffusion closures of the mean flow equations which are solved numerically, or can be substituted directly into approximate analytic expressions for the mean fields, which can then be evolved in space and time. Therefore, the present model only requires the integration of ordinary differential equations with, for example, an analytically or numerically specified acceleration. The mean fields and mechanical turbulent fields will not be reconstructed here, as they are the same as those obtained in Ref. [10]: only the new scalar turbulent fields will be considered here.

This paper is organized as follows. In Section 2 the BSDS equations are formulated using the total mixing layer width. First, in Section 2.1, the buoyancy–shear–drag equation is constructed from the sum of the individual bubble and spike equations discussed in Ref. [10]. These equations are then solved separately for general power-law acceleration-driven Rayleigh–Taylor mixing, for impulsively accelerated and Richtmyer–Meshkov mixing, and Kelvin–Helmholtz mixing analytically. The scalar variance and its dissipation rate equations are then formulated. Analytical solutions to the scalar variance equation, the calibration of the scalar variance production coefficient, the evolution equation for the molecular mixing parameter, and the mixed mass are discussed in Secs. 2.2–2.5. Analytic solutions to the coupled BSDS equations for the total mixing layer widths are derived for each instability in Section 3. The calibration of the scalar variance dissipation coefficient using the asymptotic molecular mixing parameter and scalar variance decay rate is discussed in Section 4. The analytical solutions of the general BSDS equations for the bubble and spike widths are derived in Section 5. The calibration of the scalar variance dissipation coefficient in the general case is discussed in Section 6. The model coefficients in the equations based on the total mixing layer width are calibrated in Section 7, and expressions for turbulent quantities are also provided. The coupled bubble and spike and scalar variance model equations are then solved numerically in Section 8 for representative Rayleigh–Taylor, reshocked Richtmyer–Meshkov, and Kelvin–Helmholtz mixing layer cases considered in Ref. [10] to illustrate the time-evolution of the molecular mixing parameters, scalar variances, and scalar variance dissipation rates, as well as the spatiotemporal evolution of the scalar variance, scalar variance dissipation rate, and molecular mixing profiles across the layers. Finally, a summary of the modeling methodology, principal results, conclusions, and potential further uses of the model are given in Section 9.

2. Formulation and solution of the buoyancy–shear–drag–scalar model equations

The general formulation described in Ref. [10] considered separate buoyancy–shear–drag equations for the less dense (bubble) and denser (spike) fluids. The equations were solved analytically for each type of instability, and relations between the mixing layer growth parameters and exponents and the buoyancy, shear, and drag model coefficients were used to calibrate the coefficient values so that the model would predict specified values of these parameters and exponents. This calibration methodology is the same as that used for the three- and four-equation mechanical–scalar Reynolds-averaged turbulence models for the instabilities considered here [7].

The development of the buoyancy–shear–drag model coupled to an active scalar is first illustrated for the simplified case corresponding to the total mixing layer width. The equation for the total (bubble plus spike) mixing width h is constructed by adding the bubble and spike mixing width equations derived in Ref. [10]. The resulting equation is then solved analytically for the mixing layer width for each instability case. The expressions for the mixing layer growth parameters for Rayleigh–Taylor and Kelvin–Helmholtz mixing and the growth exponent for Richtmyer–Meshkov mixing are then solved for the three model coefficients. The scalar variance, S, equation is then derived from the fluctuating scalar equation, and the scalar variance dissipation rate χ is closed either with an algebraic expression or by solving the scalar variance dissipation rate equation constructed from the S equation using scale-similarity.

Using the algebraic scalar variance dissipation rate, the general scalar variance equation is solved analytically as a functional of $h(t)$. The scalar variance is then substituted into the buoyancy and shear production terms in the mixing layer width equation (effectively generalizing the constant Atwood number to depend on the scalar variance) and the resulting equation is solved analytically for each instability case in the early- and late-time limits. In addition to considering miscible mixing with an asymptotic value of the molecular mixing parameter $\theta_{mol} \in (0,1)$, analytical solutions are also given for the limiting cases of fully-atomic miscible mixing with $\theta_{mol} = 1$ and immiscible mixing with $\theta_{mol} = 0$. Finally, the production and dissipation coefficients in the S equation are calibrated using the constant asymptotic value of the molecular mixing parameter, and the exponent of the power-law decay of the scalar variance, respectively. Calibrated model coefficients are given for the Rayleigh–Taylor, Richtmyer–Meshkov, and Kelvin–Helmholtz mixing cases used to illustrate the buoyancy–shear–drag model in Ref. [10].

This analysis is then generalized to the separate bubble and spike BSDS equations. The scalar variance terms are added to the buoyancy and shear production terms and the resulting equations are solved analytically for each instability case. The relationships between the mixing layer growth parameters and exponents and the model coefficients are solved to obtain general expressions for the model coefficients, which now depend on the molecular mixing parameter. The calibration of the scalar model coefficients is similar to that used in the total mixing layer width formulation. The model is then applied to the Rayleigh–Taylor, Richtmyer–Meshkov, and Kelvin–Helmholtz mixing cases considered in Ref. [10] and solved numerically to include molecular mixing.

The principal assumptions utilized for the model developed in Ref. [10] and extended here are:

1. the mechanical and scalar properties of the mixing layer can be described using an incompressible formulation (i.e., compressibility effects are negligible);
2. the forcing terms provide dimensionally consistent and physically reasonable representations of the physical processes operative for each instability case;
3. the mean field gradients are independent of space (they could depend on time but are constants here), and;
4. the equation for the total mixing layer width can be constructed by adding the bubble and spike width equations and assuming symmetric bubble and spike growth.

In general, there is no specific requirement that the Atwood number be small.

2.1. General total mixing layer width formulation

The effects of an active scalar on the dynamics of bubbles and spikes separately can be considered, but molecular mixing is a bulk property of a mixing layer. Therefore, the equation for the total mixing layer width is considered here first to simplify the presentation. Consider the generic bubble and spike equation (1) in Ref. [10],

$$\rho_{3-i}\,\frac{dv_{3-i}}{dt} = F_b^{3-i} + F_s^{3-i} + F_{vm}^{3-i} + F_d^{3-i} + F_{abl}^{3-i}\,, \tag{1}$$

where quantities with subscript or superscript 1 correspond to the denser fluid (spike) and quantities with subscript or superscript 2 correspond to the less dense fluid (bubble), and using Eqs. (16)–(19) and (6) in that reference for the buoyancy force, shear force, virtual mass (plus pressure) force, drag force, and ablative-stabilization force,

$$F_b^{3-i}(t) = C_b\,(\rho_1 - \rho_2)\,g_{\rm eff}(t)\,, \tag{2}$$

$$F_s^{3-i}(t) = C_s\,\frac{\rho_i^2\,\rho_{3-i}}{(\rho_i + \rho_{3-i})^2}\,\frac{(\Delta v)^2}{\ell_{3-i}(t)}\,, \tag{3}$$

$$F_{vm}^{3-i}(t) = -C_{vm}^*\,\rho_i\,\frac{dv_{3-i}}{dt}\,, \tag{4}$$

$$F_d^{3-i}(t) = -\frac{C_d}{b}\,\frac{\rho_i\,|v_{3-i}(t)|}{\ell_{3-i}(t)}\,\sqrt{\left\{\left[R_i^n\,\delta_{i1} + R_i\left(\frac{h_{3-i}}{h_i}\right)^{\beta}\delta_{i2}\right]v_{3-i}(t)\right\}^2 + (\Delta v)^2}\,, \tag{5}$$

$$F_{abl}^{3-i}(t) = -C_a\,\frac{\rho_i\,v_a\,|v_{3-i}(t)|}{\ell_{3-i}(t)}\,, \tag{6}$$

respectively, where the velocities are $v_{3-i} = d\ell_{3-i}/dt$. Summing Eq. (1) over $i = 1$ and 2, taking $v_{3-i}(t) = (1/2)\,d\ell/dt = v(t)/2$ and $\ell_{3-i}(t) = \ell(t)/2$, and with the new buoyancy, shear, drag, and ablation coefficient definitions

$$C_b^* = \frac{4\,C_b}{1 + C_{vm}^*}\,,\; C_s^* = \frac{C_s}{1 + C_{vm}^*}\,,\; C_d^* = \frac{2\,C_d}{b\,(1 + C_{vm}^*)}\,,\; C_a^* = \frac{2\,C_a}{1 + C_{vm}^*}\,, \tag{7}$$

respectively, $\rho_1\rho_2/(\rho_1 + \rho_2)^2 = (1 - At^2)/4$, density Atwood number $At = (\rho_1 - \rho_2)/(\rho_1 + \rho_2) > 0$, ratio of bubble or spike density to the total density $R_i = \rho_i/(\rho_i + \rho_{3-i})$, and effective acceleration (a power-law for Rayleigh–Taylor mixing with $\theta_{RT} > 0$ and an impulse with change in velocity of the interface Δv_s)

$$g_{\rm eff}(t) = \begin{cases} g_0\left(\frac{t}{t_0}\right)^{\theta_{RT}-2} & \text{Rayleigh–Taylor} \\ \Delta v_s\,\delta(t) & \text{Richtmyer–Meshkov}\,, \end{cases} \tag{8}$$

it follows that the general buoyancy–shear–drag equation for the mixing layer width $\ell(t) = h(t)$ of all three instabilities is (redefining $R_1 \to 2^{1/n}R_1$ and $R_2 \to 2R_2$ and taking $\beta = 0$ in order to retain the conventional form of the drag term)

$$\begin{aligned}\frac{d^2h}{dt^2} &= C_b^*\,g_{\rm eff}(t)\,At + C_s^*\left(1 - At^2\right)\frac{(\Delta v)^2}{h(t)} \\ &\quad - \frac{C_d^*}{\rho_1 + \rho_2}\,\frac{|v(t)|}{h(t)} \\ &\quad \times\left[\rho_1\sqrt{\left[R_1^n\,v(t)\right]^2 + (\Delta v)^2} + \rho_2\sqrt{[R_2\,v(t)]^2 + (\Delta v)^2}\right] \\ &\quad - \overline{\nu}\,\frac{v(t)}{h(t)^2} - C_a^*\,\frac{v_a\,v(t)}{h(t)}\,,\end{aligned} \tag{9}$$

where a viscous dissipation term has also been included in Eq. (9), and $\overline{\nu} = (\nu_1 + \nu_2)/2$ is the average mixture kinematic viscosity. Here, $h(t)$ is directed normal to the interface separating the fluids, and can be interpreted as the average width of a mixing layer developing from a two- or three-dimensional flow with multimode initial perturbations. Unlike the general bubble and spike equations, this equation for the total mixing layer width is independent of the virtual mass coefficient C_{vm}^* and geometrical factor b. Later, the ablation velocity, v_a, needed to describe ablative Rayleigh–Taylor and Richtmyer–Meshkov instability stabilization in inertial confinement fusion will be set to zero.

The R_i terms in the drag term empirically introduce a possible bubble to spike density ratio dependence, but as will be assumed later, typically $R_i = 1$ (n is a fitting exponent as briefly discussed in Ref. [10]). The motivation for considering power-law acceleration-driven Rayleigh–Taylor mixing is discussed in detail elsewhere [9]; $\theta_{RT} = 2$ corresponds to the canonical constant acceleration case. Note that $g_{\rm eff}(t)$ for Rayleigh–Taylor mixing decreases with increasing time (i.e., corresponding to a *deceleration*) for $\theta_{RT} \in (0, 2)$. Also, the power-law Rayleigh–Taylor acceleration allows for a description of Richtmyer–Meshkov instability for $\theta_{RT} \le 0$, as discussed in detail elsewhere in the context of a statistical bubble merger model [17], zero-dimensional, reduced turbulence models [16], and more recently in the momentum model [18].

In this formulation considering only the total (bubble plus spike) mixing layer width, there is no characterization of the Atwood number-dependent asymmetry between the bubble and spike widths. The momentum model, which is closely related to the buoyancy–drag model, was recently applied to Rayleigh–Taylor mixing in the linear, nonlinear, and turbulent regimes generated by a power-law acceleration $g_{\rm eff}(t) = Gt^a$ [19]. Analytical solutions were derived and further analyzed in the context of supernova remnants.

2.1.1. Analytic solutions of the buoyancy–shear–drag equation and model calibration

Substitute the general power-law total mixing layer width ($\theta_h > 0$)

$$h(t) = A_h\,t^{\theta_h} \tag{10}$$

into Eq. (9):

$$\begin{aligned}\theta_h\,(\theta_h - 1)\,A_h\,t^{\theta_h - 2} &= C_b^*\,g_{\rm eff}(t)\,At + C_s^*\left(1 - At^2\right)\frac{(\Delta v)^2}{A_h}\,t^{-\theta_h} \\ &\quad - \frac{C_d^*}{\rho_1 + \rho_2}\,\frac{|\theta_h|}{t} \\ &\quad \times\left[\rho_1\sqrt{\left(R_1^n\,\theta_h\,A_h\,t^{\theta_h - 1}\right)^2 + (\Delta v)^2}\right. \\ &\quad \left. + \rho_2\sqrt{\left(R_2\,\theta_h\,A_h\,t^{\theta_h - 1}\right)^2 + (\Delta v)^2}\right] \\ &\quad - \overline{\nu}\,\frac{\theta_h}{A_h}\,t^{-\theta_h - 1} - C_a^*\,\frac{v_a\,\theta_h}{t}\,.\end{aligned} \tag{11}$$

For Rayleigh–Taylor ($C_s^* = \Delta v = \overline{\nu} = C_a^* = 0$), Richtmyer–Meshkov ($C_s^* = g_0 = \Delta v = \overline{\nu} = C_a^* = 0$), and Kelvin–Helmholtz ($C_b^* = R_i = \overline{\nu} = C_a^* = 0$)

instability, the prefactors and power-law exponents are

$$A_h = \alpha\, At\, g_0\, t_0^{2-\theta_{RT}} \quad , \quad \theta_h = \theta_{RT}\,, \tag{12}$$

$$A_h = h_0 \left(\frac{\Delta v_s\, At^+}{\theta\, h_0} \right)^{\theta} \quad , \quad \theta_h = \theta\,, \tag{13}$$

$$A_h = \delta\, |\Delta v| \quad , \quad \theta_h = 1\,, \tag{14}$$

respectively, corresponding to the late-time mixing layer widths

$$h(t) = \alpha\, At\, g_{\text{eff}}(t)\, t^2 = \alpha\, At\, g_0\, t_0^2 \left(\frac{t}{t_0} \right)^{\theta_{RT}} , \tag{15}$$

$$h(t) = h_0 \left(\frac{\Delta v_s\, At^+\, t}{\theta\, h_0} \right)^{\theta} , \tag{16}$$

$$h(t) = \delta\, |\Delta v|\, t\,, \tag{17}$$

where the postshock Atwood number At^+ is included in the Richtmyer–Meshkov width such that the initial velocity is $dh/dt|_{t=0} = \Delta v_s At^+$ when the width is expressed as $h(t) = h_0\left[1 + \Delta v_s At^+ t/(\theta h_0)\right]^{\theta}$ so that $h(0) = h_0$.

With these substitutions it follows that

$$\theta_{RT}\,(\theta_{RT} - 1)\,\alpha = C_b^* - \frac{\theta_{RT}^2\, C_d^*}{\rho_1 + \rho_2} \left(\rho_1\, R_1^n + \rho_2\, R_2 \right) \alpha\,,$$

$$\theta - 1 = -\frac{C_d^*\, \theta}{\rho_1 + \rho_2} \left(\rho_1\, R_1^n + \rho_2\, R_2 \right),$$

$$0 = \frac{C_s^*}{\delta} \left(1 - At^2 \right) - C_d^*\,.$$

Solving these algebraic equations for α, θ, and δ gives the general expressions for the Rayleigh–Taylor growth parameter, Richtmyer–Meshkov growth exponent, and Kelvin–Helmholtz growth parameter

$$\alpha(C_b^*, C_d^*; R_i) = \frac{C_b^*}{\theta_{RT}\,(\theta_{RT} - 1) + \frac{\theta_{RT}^2\, C_d^*}{\rho_1 + \rho_2} \left(\rho_1\, R_1^n + \rho_2\, R_2 \right)} ,$$

$$\theta(C_d^*; R_i) = \frac{1}{1 + \frac{C_d^*}{\rho_1 + \rho_2} \left(\rho_1\, R_1^n + \rho_2\, R_2 \right)} ,$$

$$\delta(C_s^*, C_d^*) = \frac{C_s^*}{C_d^*} \left(1 - At^2 \right),$$

respectively. These relations provide three equations for the three coefficients C_b^*, C_d^*, and C_s^*. Note that the power-law widths (10) correspond to self-similar, fully-developed turbulent mixing and do not account for transition to turbulence.

To simplify the solutions, let $R_1 = R_2 = 1$, so that

$$\alpha(C_b^*, C_d^*) = \frac{C_b^*}{\theta_{RT}\,(\theta_{RT} - 1) + \theta_{RT}^2\, C_d^*} , \tag{18}$$

$$\theta(C_d^*) = \frac{1}{1 + C_d^*}. \tag{19}$$

Solving these equations gives the coefficients as a function of the growth parameters and exponent:

$$C_b^*(\alpha, \theta) = \frac{\alpha\, \theta_{RT}\,(\theta_{RT} - \theta)}{\theta} , \tag{20}$$

$$C_d^*(\theta) = \frac{1 - \theta}{\theta} , \tag{21}$$

$$C_s^*(\delta, \theta) = \frac{\delta}{1 - At^2}\, \frac{1 - \theta}{\theta} = \frac{\delta}{1 - At^2}\, C_d^*(\theta) \tag{22}$$

($\theta_{RT} > \theta$ and $At \neq 1$). It is clear that the value of C_b^* increases with increasing θ_{RT}. The calibration of the model coefficients in the buoyancy–shear–drag equations for the bubble and spike widths separately is discussed in Section 5.

2.1.2. *Coupling the scalar variance equation to the buoyancy–shear–drag equation*

For Rayleigh–Taylor mixing in the Boussinesq approximation, Schilling and Mueschke [20, 21] discussed the formulation and application of three- and four-equation mechanical–scalar Reynolds-averaged turbulence models motivated by consideration of both experimental and direct numerical simulation data. The extension of the buoyancy–shear-drag model developed in Ref. [10] to include scalar fluctuations is analogous to Reynolds-averaged modeling, except that the models here include active scalars and do not require the Boussinesq approximation.

The scalar variance equation. Consider nonreactive, binary fluid mixing at molecular or atomic scales. Small fluctuations in scalar quantities such as the (heavy or light) mass fraction, density, or concentration are produced through gradients of these scalars near and across the interface separating fluids with different densities. Consider the general incompressible scalar transport equation

$$\frac{\partial \phi}{\partial t} + \mathbf{v} \cdot \nabla \phi = \overline{D}\, \partial^2 \phi\,, \tag{23}$$

where ∂^2 is the Laplacian and $\overline{D} = (D_1 + D_2)/2$ is the average mixture scalar diffusivity. Substituting the Reynolds decompositions of mean (denoted by an overbar) plus fluctuating (denoted by a prime) fields $\mathbf{v} = \overline{\mathbf{v}} + \mathbf{v}'$ and $\phi = \overline{\phi} + \phi'$ into this equation and Reynolds averaging the resulting equation using the standard averaging rules (e.g., $\overline{v'} = \overline{\phi'} = 0$) gives the mean scalar equation

$$\frac{\partial \overline{\phi}}{\partial t} + \overline{\mathbf{v}} \cdot \nabla \overline{\phi} + \overline{\mathbf{v}' \cdot \nabla \phi'} = \overline{D}\, \partial^2 \overline{\phi}\,. \tag{24}$$

Once again substituting the Reynolds decompositions of the velocity and scalar into the unaveraged equation (23) and subtracting the mean equation (24) gives the fluctuating scalar transport equation

$$\frac{\partial \phi'}{\partial t} + \mathbf{v}' \cdot \nabla \overline{\phi} + \overline{\mathbf{v}} \cdot \nabla \phi' + \mathbf{v}' \cdot \nabla \phi' - \overline{\mathbf{v}' \cdot \nabla \phi'} = \overline{D}\, \partial^2 \phi'\,. \tag{25}$$

Multiplying this equation by ϕ', Reynolds averaging the resulting equation, defining $d/dt = \partial/\partial t + \mathbf{v} \cdot \nabla$, and defining the scalar variance $S = \overline{\phi'^2}$ gives the unclosed equation

$$\frac{dS}{dt} = -2\, \overline{\phi'\, \mathbf{v}'} \cdot \nabla \overline{\phi} - \overline{\phi'\, \mathbf{v}' \cdot \nabla \phi'^2} + 2\, \overline{D}\, \overline{\phi'\, \partial^2 \phi'}\,. \tag{26}$$

Finally, the scalar variance equation (in a reference frame in which $\overline{\mathbf{v}} = 0$) is closed by taking the mean scalar gradient $\nabla \overline{\phi} \sim \Delta\phi/\ell$, assuming the gradient-diffusion closure of the scalar–velocity correlation $\overline{\phi' \mathbf{v}'} = -\left(C_p/4\right) D_t \nabla \overline{\phi}$ using a turbulent diffusivity $D_t \propto v\ell$, using $\overline{\phi'\, \partial^2 \phi'} = \partial^2 S/2 - \overline{(\nabla \phi')^2}$, and assuming homogeneity (so that the term $\overline{\phi'\, \mathbf{v}' \cdot \nabla \phi'^2}$, which would be modeled as a turbulent diffusion term in a Reynolds-averaged model, is zero):

$$\begin{aligned} \frac{dS}{dt} &= \frac{C_p}{2}\, v\, \ell \left(\nabla \overline{\phi} \right)^2 - 2\chi + \overline{D}\, \partial^2 S \\ &= \frac{C_p}{2}\, \frac{v}{\ell}\, (\Delta \phi)^2 - 2\chi + \overline{D}\, \frac{S}{\ell^2}\,, \end{aligned} \tag{27}$$

where the scalar variance dissipation rate (which can be interpreted as a *mixing rate* with units of inverse time if S is dimensionless) is

$$\chi = \overline{D}\, \overline{(\nabla \phi')^2}\,, \tag{28}$$

ℓ is the lengthscale over which the mean gradients change, and C_p is a dimensionless coefficient that will be calibrated later in Section 2.3. If $C_p = 0$ there is no scalar flux and no production of scalar variance, only decay as mixing progresses. In this case, the suppression of scalar fluctuations is consistent with *immiscible* mixing (i.e., interpenetration of the fluids without scalar mixing at molecular or atomic scales).

A similar model was previously formulated and analytically solved for Rayleigh–Taylor mixing with an active scalar, based on a temperature fluctuation evolution equation $dT'/dt = -\chi\,(\nabla T')^2/\overline{T} \sim -\left(v\ell/\overline{T}\right)(T'/\ell)^2$ [22]. However, a temperature production term was not included.

With the velocity $v = dh/dt$ and using Eq. (10), the instability timescale can be defined by

$$\tau_h(t) = \frac{h(t)}{v(t)} = \frac{t}{\theta_h}\,, \tag{29}$$

differing only in the value of the power-law exponent θ_h. In a K–ϵ-based turbulence model [7], the mechanical turbulent mixing timescale is $\tau_m = K/\epsilon$. The large-scale turbulent kinetic production scales as $P_K = C_\epsilon K^{3/2}/\ell$ (where ℓ is a turbulent lengthscale of the order of the mixing layer width h and C_ϵ is a dimensionless coefficient), which can be rewritten as

$$\epsilon = \frac{C_\epsilon}{P_K/\epsilon}\,\frac{K^{3/2}}{\ell} = C_d^*\,\frac{K^{3/2}}{\ell}\,,$$

such that the P_K/ϵ factor has been absorbed into the drag coefficient C_d^*. In general, $P_K/\epsilon > 1$ and is time-dependent in hydrodynamic instability-induced turbulent flows, but becomes a constant in a late-time, self-similar state; see Ref. [20] for the case of Rayleigh–Taylor instability for example. With $K \sim v^2$ and $\epsilon \sim v^3/\ell \sim K^{3/2}/\ell$, it follows that $\tau_m = \ell/v$, which is equivalent to the instability timescale τ_h (29) for $\ell = h$.

The scalar turbulent mixing timescale is $\tau_s = S/(2\chi)$, so that the mechanical-to-scalar timescale ratio is

$$R = \frac{\tau_m}{\tau_s} = \frac{2\,\ell}{v}\,\frac{\chi}{S} \tag{30}$$

analogous to the expression $R = 2K\chi/(\epsilon S)$ in Reynolds-averaged models [7].

The scalar variance dissipation rate equation. In the simplest case, χ can be modeled algebraically as

$$\chi(t) = C_\chi\,\frac{v(t)\,S(t)}{\ell(t)}\,, \tag{31}$$

analogously to the three-equation Reynolds-averaged case [7], where C_χ is the dimensionless scalar variance dissipation rate coefficient (which will be calibrated later in Section 4). With $\ell = h$ and Eq. (29),

$$\chi(t) = C_\chi\,\frac{\theta_h\,S(t)}{t}\,. \tag{32}$$

Alternatively, rather than deriving a complicated equation directly from the fluctuating scalar equation (25) (which must be closed in any case), an evolution equation for χ can be empirically derived by multiplying each term in the S equation by the inverse scalar mixing timescale χ/S and an associated dimensionless coefficient:

$$\frac{d\chi}{dt} = \frac{C_{\chi0}}{4}\,\frac{v}{\ell}\,\frac{\chi}{S}\,(\Delta\phi)^2 + C_{\chi3}\,\frac{v\chi}{\ell} - C_{\chi2}\,\frac{\chi^2}{S} + \overline{D}\,\frac{\chi}{\ell^2}\,. \tag{33}$$

Alternatively, it is more conventional to use the inverse mechanical mixing timescale $\epsilon/K = v/\ell$ to form this equation:

$$\frac{d\chi}{dt} = \frac{C_{\chi0}}{4}\,\frac{v^2}{\ell^2}\,(\Delta\phi)^2 + C_{\chi3}\,\frac{v^2\,S}{\ell^2} - C_{\chi2}\,\frac{v\chi}{\ell} + \overline{D}\,\frac{v\,S}{\ell^3}\,. \tag{34}$$

This equation is analogous to the scalar variance dissipation rate transport equation in the four-equation K–ϵ–S–χ Reynolds-averaged model [7], the motivation for and analysis of which is discussed in detail elsewhere in the context of modeling Rayleigh–Taylor mixing [20, 21]. Equations (33) and (34) require the specification of three dimensionless model coefficients $C_{\chi0}$, $C_{\chi2}$, and $C_{\chi3}$ (a simpler model can be obtained by taking $C_{\chi3} = 0$). Note that the right sides of Eqs. (33) and (34) differ by a factor of $R/2$.

The coupled buoyancy–shear–drag–scalar equations. Define $\Delta\phi = \phi_1 - \phi_2$ and the mean scalar $\overline{\phi} = (\phi_1 + \phi_2)/2$ so that the constant 'generalized scalar Atwood number' is

$$At_\phi = \frac{\Delta\phi}{2\,\overline{\phi}}\,. \tag{35}$$

With this definition, Eqs. (27) and (33) become

$$\frac{dS}{dt} = 2\,C_p\,\overline{\phi}^2\,At_\phi^2\,\frac{v(t)}{\ell(t)} - 2\chi(t) + \overline{D}\,\frac{S(t)}{\ell(t)^2}\,, \tag{36}$$

$$\frac{d\chi}{dt} = C_{\chi0}\,\overline{\phi}^2\,At_\phi^2\,\frac{v(t)\chi(t)}{\ell(t)\,S(t)} + C_{\chi3}\,\frac{v(t)\chi(t)}{\ell(t)} - C_{\chi2}\,\frac{\chi(t)^2}{S(t)} + \overline{D}\,\frac{\chi(t)}{\ell(t)^2}\,. \tag{37}$$

In analogy with Reynolds-averaged models [7], the scalar variance production-to-dissipation ratio is

$$\frac{P_S}{D_S} = C_p\,\overline{\phi}^2\,At_\phi^2\,\frac{v}{\ell\chi} = \frac{C_p}{C_\chi}\,\frac{\overline{\phi}^2\,At_\phi^2}{S}\,, \tag{38}$$

which is proportional to the ratio of the production and dissipation coefficients C_p/C_χ, and the scalar variance dissipation rate production-to-destruction ratio is

$$\frac{P_\chi}{D_\chi} = \frac{C_{\chi0}\,\overline{\phi}^2\,At_\phi^2 + C_{\chi3}\,S}{C_{\chi2}}\,\frac{v}{\ell\chi}\,. \tag{39}$$

Define the normalized scalar variance and the normalized scalar variance dissipation rate

$$\Xi(t) = \frac{\overline{\phi'^2}}{\overline{\phi}^2} = \frac{S(t)}{\overline{\phi}^2}\quad,\quad \Sigma(t) = \frac{\chi(t)}{\overline{\phi}^2}$$

respectively, so that the coupled nonlinear BSDS model equations for miscible fluids are [using Eq. (37) and $\ell = h$ in the scalar equations]

$$\frac{d^2h}{dt^2} = C_b^*\,g_{\rm eff}(t)\,At\,\sqrt{\Xi(t)} + C_s^*\left[1 - At^2\,\Xi(t)\right]\frac{(\Delta v)^2}{h(t)} - C_d^*\,\frac{|v(t)|}{h(t)}\,\sqrt{v(t)^2 + (\Delta v)^2} - \overline{\nu}\,\frac{v(t)}{h(t)^2}\,, \tag{40}$$

$$\frac{d\Xi}{dt} = 2\,C_p\,At_\phi^2\,\frac{v(t)}{h(t)} - 2\,\Sigma(t) + \overline{D}\,\frac{\Xi(t)}{h(t)^2}\,, \tag{41}$$

$$\frac{d\Sigma}{dt} = C_{\chi0}\,At_\phi^2\,\frac{v(t)\chi(t)}{h(t)\,S(t)} + C_{\chi3}\,\frac{v(t)\,\Sigma(t)}{h(t)} - C_{\chi2}\,\frac{\Sigma(t)\chi(t)}{S(t)} + \overline{D}\,\frac{\Sigma(t)}{h(t)^2} \tag{42}$$

with dimensionless coefficients $\{C_b^*, C_s^*, C_d^*, C_p, C_{\chi0}, C_{\chi2}, C_{\chi3}\} > 0$. The buoyancy term in Eq. (40) is motivated by the form of the buoyancy term in the momentum equation describing incompressible Rayleigh–Taylor instability in the Boussinesq approximation [23–25], which introduces a fluctuating scalar $\phi' \approx \sqrt{\overline{\phi'^2}} = \sqrt{S}$ (e.g., concentration or temperature) multiplying $g_{\rm eff}At$. However, note that the relationship $\rho'/\rho_0 = -\beta T'$ (where β is the thermal expansion coefficient) between the density and temperature fluctuation results in the buoyancy term changing sign in the momentum equation (and these fluctuations can be both positive and negative), whereas the buoyancy term in the BSDS equation (40) must be positive in order for the mixing layer to grow in the unstable case.

Introducing

$$\Theta(t) = \sqrt{\Xi(t)}\,, \tag{43}$$

it follows that

$$\frac{d\Theta}{dt} = \frac{1}{2\sqrt{\Xi}}\,\frac{d\Xi}{dt} = \frac{1}{2\,\Theta}\,\frac{d\Xi}{dt}\,,$$

so that the mechanical and scalar equations (40)–(42) can be expressed in

the form

$$\frac{d^2h}{dt^2} = C_b^*\, g_{\rm eff}(t)\, At\, \Theta(t) + C_s^* \left[1 - At^2\, \Theta(t)^2\right] \frac{(\Delta v)^2}{h(t)} - C_d^* \frac{|v(t)|}{h(t)} \sqrt{v(t)^2 + (\Delta v)^2} - \overline{\nu}\, \frac{v(t)}{h(t)^2}\,, \tag{44}$$

$$\frac{d\Theta}{dt} = C_p\, At_\phi^2\, \frac{v(t)}{\Theta(t)\, h(t)} - \frac{\Sigma(t)}{\Theta(t)} + \frac{\overline{D}}{2}\, \frac{\Theta(t)}{h(t)^2}\,, \tag{45}$$

$$\frac{d\Sigma}{dt} = C_{\chi 0}\, At_\phi^2\, \frac{v(t)\, \Sigma(t)}{h(t)\, \Theta(t)^2} + C_{\chi 3}\, \frac{v(t)\, \Sigma(t)}{h(t)} - C_{\chi 2}\, \frac{\Sigma(t)^2}{\Theta(t)^2} + \overline{D}\, \frac{\Sigma(t)}{h(t)^2}\,, \tag{46}$$

from which it is apparent that Θ is an active scalar that modifies the buoyancy and shear production terms in the h equation. In Eq. (44), $At\, \Theta(t) = At_{\rm eff}(t)$ can be interpreted as a time-dependent effective density Atwood number. For the algebraic model (31),

$$\Sigma(t) = C_\chi\, \frac{v(t)\, \Theta(t)^2}{h(t)} \tag{47}$$

and Eq. (45) becomes

$$\frac{d\Theta}{dt} = C_p\, At_\phi^2\, \frac{v(t)}{\Theta(t)\, h(t)} - C_\chi\, \frac{v(t)\, \Theta(t)}{h(t)} + \frac{\overline{D}}{2}\, \frac{\Theta(t)}{h(t)^2}\,. \tag{48}$$

The production and destruction/molecular diffusion terms in the Θ equation are proportional to $1/\Theta$ and Θ, respectively.

Using the previous definitions, the scalar variance and its dissipation rate can be expressed as

$$S(t) = \overline{\phi}^2\, \Xi(t) = \overline{\phi}^2\, \Theta(t)^2 \quad , \quad \chi(t) = \overline{\phi}^2\, \Sigma(t)\,,$$

and the scalar turbulent mixing timescale using these variables is $\tau_s = S/(2\chi) = \Theta^2/(2\Sigma) = \Xi/(2\Sigma)$. It may be possible to obtain analytical solutions to Eqs. (44)–(46) in certain limiting cases or under particular approximations, or they may be solved numerically with specified initial conditions. Henceforth, only the model using the algebraic closure (31) will be considered [i.e., Eqs. (44) and (48)] in order to obtain analytical solutions and simplify the model calibration.

Early time solution of the buoyancy–shear–drag equation. At very early times when molecular viscous dissipation dominates, Eq. (44) reduces to

$$\frac{dv}{dt} = -\overline{\nu}\, \frac{v(t)}{h(t)^2}\,. \tag{49}$$

Substituting Eq. (10) into this equation gives

$$\theta_h\, (\theta_h - 1)\, A_h\, t^{\theta_h - 2} = -\frac{\overline{\nu}\, \theta_h}{A_h}\, t^{-\theta_h - 1}\,,$$

which is solved by $\theta_h = 1/2$ and $A_h = \sqrt{2\overline{\nu}}$ so that (introducing the average Schmidt number $\overline{Sc} = \overline{\nu}/\overline{D}$),

$$h(t) = \sqrt{2\, \overline{\nu}\, t} = \sqrt{2\, \overline{Sc}\, \overline{D}\, t}\,, \tag{50}$$

which describes the expected slow diffuse growth in time of the very early-time mixing layer width due to molecular dissipation/diffusion.

2.2. Analytical solutions for the scalar variance

The equation for the normalized scalar variance (48) with $\overline{D} = 0$ can be solved analytically for $C_p \neq 0$ and for $C_p = 0$. The physical significance of these solutions in discussed in Section 2.3.

2.2.1. Solutions for $C_p \neq 0$

The formal solution of Eq. (48) with $\Theta(0) = \Theta_0$ and $\overline{D} = 0$ is ($C_\chi \neq 0$)

$$\Theta(t) = \sqrt{\frac{C_p\, At_\phi^2}{C_\chi} + \left(\Theta_0^2 - \frac{C_p\, At_\phi^2}{C_\chi}\right) \left[\frac{h_0}{h(t)}\right]^{2C_\chi}}\,, \tag{51}$$

so that the normalized scalar variance is

$$\frac{S(t)}{\overline{\phi}^2} = \Theta(t)^2 = \frac{C_p\, At_\phi^2}{C_\chi} + \left(\Theta_0^2 - \frac{C_p\, At_\phi^2}{C_\chi}\right) \left[\frac{h_0}{h(t)}\right]^{2C_\chi}\,. \tag{52}$$

As $h(t)$ very rapidly attains its self-similar form, the second term rapidly decreases, and

$$\lim_{t \uparrow \infty} \Theta(t) = \sqrt{\frac{S(t)}{\overline{\phi}^2}} \downarrow At_\phi \sqrt{\frac{C_p}{C_\chi}}\,. \tag{53}$$

These expressions depend on the ratio C_p/C_χ (i.e., on the relative importance of production and destruction) and not on C_p and C_χ separately.

2.2.2. Solutions for $C_p = 0$

Consider $C_p = 0$. The formal power-law solution of

$$\frac{d \ln \Theta}{dt} = -C_\chi\, \frac{v(t)}{h(t)} = -C_\chi\, \frac{d \ln h}{dt} \tag{54}$$

is

$$\Theta(t) = \Theta(0) \exp\left[-C_\chi \int_{t_0}^{t} d \ln h(t')\right] = \Theta(0) \exp\left\{-C_\chi \ln\left[\frac{h(t)}{h(t_0)}\right]\right\} = \Theta_0 \left[\frac{h(t)}{h_0}\right]^{-C_\chi} \tag{55}$$

with initial values $h_0 = h(0)$ and $\Theta_0 = \Theta(0)$, and $\Theta \downarrow 0$ as $t \uparrow \infty$. The corresponding normalized scalar variance is

$$\frac{S(t)}{\overline{\phi}^2} = \Theta(t)^2 = \Theta_0^2 \left[\frac{h_0}{h(t)}\right]^{2C_\chi}\,. \tag{56}$$

As $h(t)$ rapidly increases, $S(t)/\overline{\phi}^2 \downarrow 0$. The analytical solutions (51) and (55) depend parametrically on $h(t)/h_0$. Note that if $C_p = C_\chi = 0$, then Θ is a constant because S is a constant ($dS/dt = 0$).

2.3. Calibration of the scalar variance production coefficient C_p

In general, the calibration of C_χ is specific to each instability (and uses their analytical solutions), and is discussed later in Section 4, where a universal calibration of C_χ is also presented. The coefficient C_p can be calibrated as follows.

Using Eq. (51), the general expression for the molecular mixing parameter (analogous to that used in water channel Rayleigh–Taylor experiments and simulations [26, 27]) is

$$\theta_m(t) = 1 - \frac{4\, S(t)}{(\Delta\phi)^2} = 1 - \frac{S(t)}{At_\phi^2\, \overline{\phi}^2} = 1 - \frac{\Theta(t)^2}{At_\phi^2} = 1 - \frac{C_p}{C_\chi} - \left(\frac{\Theta_0^2}{At_\phi^2} - \frac{C_p}{C_\chi}\right) \left[\frac{h_0}{h(t)}\right]^{2C_\chi} \tag{57}$$

with asymptotic value in the self-similar regime

$$\theta_m(\infty) \equiv \theta_{mol} = 1 - \frac{S(\infty)}{At_\phi^2\, \overline{\phi}^2} = 1 - \frac{C_p}{C_\chi}\,, \tag{58}$$

so that the production and dissipation coefficients are linearly related by

$$C_p = (1 - \theta_{mol})\, C_\chi \,. \tag{59}$$

Clearly, the inequality $0 \le C_p \le C_\chi$ must be satisfied so that $\theta_{mol} \in [0, 1]$. Equation (57) shows that $\theta_m(t)$ is a functional of $h(t)$. Using the previous expressions, the scalar variance production-to-dissipation ratio (38) can be expressed as

$$\frac{P_S}{D_S} = \frac{A t_\phi^2}{\Theta(t)^2}\,(1 - \theta_{mol}) = \frac{1 - \theta_{mol}}{1 - \theta_m(t)}\,, \tag{60}$$

showing that $P_S/D_S \to 1$ as $\theta_m(t) \to \theta_{mol}$.

The model developed here can describe two other mixing limits:

- *miscible fully-atomic mixing* corresponding to

$$C_p = 0 \;\;,\;\; \theta_{mol} = 1 \;\;,\;\; S(\infty) = 0 \tag{61}$$

- *immiscible mixing* corresponding to

$$C_p = C_\chi \;\;,\;\; \theta_{mol} = 0 \;\;,\;\; S(\infty) = A t_\phi^2\, \overline{\phi}^2 \,. \tag{62}$$

Fully-atomic mixing results when the scalar fluctuations (and therefore scalar variance) approach zero under the action of dissipation with no production, $P_S/D_S = 0$, and Eq. (57) reduces to

$$\theta_m(t) = 1 - \frac{\Theta_0^2}{A t_\phi^2}\left[\frac{h_0}{h(t)}\right]^{2C_\chi} \tag{63}$$

with $\theta_m(\infty) = \theta_{mol} = 1$. This solution also directly follows from Eq. (51) by setting $C_p = 0$. Immiscible mixing results when the scalar variance has its constant maximum value and does not decrease, $P_S/D_S = 1/[1 - \theta_m(t)]$, and Eq. (57) reduces to

$$\theta_m(t) = \left(1 - \frac{\Theta_0^2}{A t_\phi^2}\right)\left[\frac{h_0}{h(t)}\right]^{2C_\chi} \tag{64}$$

with $\theta_m(\infty) = \theta_{mol} = 0$ and $P_S/D_S \downarrow 1$. Solutions of the models for these two limiting cases will also be given for each instability case in Section 3.

2.4. Molecular mixing parameter evolution equation

As $h(t)$ increases, $\Theta(t)$ and $S(t)$ decrease and $\theta_m(t)$ increases, and approach their asymptotic values. It follows from Eq. (57) that the initial molecular mixing parameter is

$$\theta_m(0) \equiv \theta_0 = 1 - \frac{S(0)^2}{A t_\phi^2\, \overline{\phi}^2} = 1 - \frac{\Theta_0^2}{A t_\phi^2} < 1 \,. \tag{65}$$

Differentiating Eq. (57) with respect to time gives the molecular mixing parameter evolution equation

$$\begin{aligned} \frac{d\theta_m}{dt} &= 2\, C_\chi \left(\frac{\Theta_0^2}{A t_\phi^2} - \frac{C_p}{C_\chi}\right)\left[\frac{h_0}{h(t)}\right]^{2C_\chi} \frac{d\ln h}{dt} \\ &= 2\, C_\chi \left[1 - \frac{C_p}{C_\chi} - \theta_m(t)\right] \frac{d\ln h}{dt} \\ &= 2\, \theta_h\, C_\chi\, \frac{\theta_{mol} - \theta_m(t)}{t} \,, \end{aligned} \tag{66}$$

which is a relaxation model [the last expression uses the self-similar mixing layer width (10)] with solution ($t_0 > 0$)

$$\theta_m(t) = \theta_{mol} + (\theta_0 - \theta_{mol})\left(\frac{t_0}{t}\right)^{2\theta_h C_\chi} \,, \tag{67}$$

which is an alternative form of the last expression in Eq. (57) with $t_0 = (h_0/A_h)^{1/\theta_h}$. When the BSDS equations are integrated numerically, $h(t)$ can be directly substituted into Eq. (57) or the first expression in Eq. (66) can be integrated.

As θ_m depends on θ_h through the power-law exponent in Eq. (67), this expression is different for each instability. Clearly, $\theta_m(t) \downarrow \theta_{mol}$ as $t \uparrow \infty$. This simple model does not describe the early transitional decrease of $\theta_m(t)$ to a minimum value, followed by an increase observed in experiments [26, 28, 29] and numerical simulations [12, 27, 30] because $h(t)$ [Eq. (10)] describes an initially fully-turbulent state.

2.5. Mixed mass evolution

Generalizing the self-similar mixed mass, Eq. (74) in Ref. [9] to include a time-dependent molecular mixing parameter $\theta_m(t)$, an averaged (areal) mixed mass can be defined for the BSDS model as

$$\mathcal{M}_h(t) = \rho_0\, \theta_m(t)\, h(t) \approx A_h\, \rho_0 \left[\theta_{mol} + (\theta_0 - \theta_{mol})\left(\frac{t_0}{t}\right)^{2\theta_h C_\chi}\right] t^{\theta_h} \tag{68}$$

for each instability, where $\rho_0 = (\rho_1 + \rho_2)/2$ is the average density. Asymptotically,

$$\lim_{t\uparrow\infty} \mathcal{M}_h(t) = \rho_0\, \theta_{mol}\, h(t) \le \rho_0\, h(t) \,,$$

which shows that the late-time (areal) mixed mass is simply the average density multiplied by the mixing layer width, modulated by the asymptotic value of the molecular mixing parameter (with the last inequality a consequence of $\theta_{mol} \le 1$). If the BSDS equations are solved for a combined instability numerically, then $h(t)$ would have a different evolution than Eq. (10) for a particular single instability.

3. Analytic solutions of the buoyancy–shear–drag–scalar model equations for each instability in the total mixing layer width formulation

The analytic solutions of the buoyancy–shear–drag–scalar model equations depending only on the total mixing layer width are derived here for power-law acceleration-driven Rayleigh–Taylor, Richtmyer–Meshkov, and Kelvin–Helmholtz mixing.

For any instability, substituting the general power-law (10) into Eq. (44) gives

$$\begin{aligned} \theta_h\,(\theta_h - 1)\, A_h\, t^{\theta_h - 2} = {} & C_b^*\, g_{\rm eff}(t)\, A t\, \Theta(t) + C_s^* \left[1 - A t^2\, \Theta(t)^2\right] \frac{(\Delta v)^2}{A_h}\, t^{-\theta_h} \\ & - \frac{C_d^*\, |\theta_h|}{t} \sqrt{(\theta_h\, A_h\, t^{\theta_h - 1})^2 + (\Delta v)^2} - \overline{\nu}\, \frac{\theta_h}{A_h}\, t^{-\theta_h - 1} \,, \end{aligned} \tag{69}$$

where $A t\, \Theta(t) = A t_{\rm eff}(t)$ can be interpreted as a time-dependent effective density Atwood number. This equation will be reduced for each instability case below to determine the power-law exponent θ_h of the mixing layer width and the coefficient A_h for the active scalar case.

3.1. Power-law acceleration-driven Rayleigh–Taylor mixing

Analytic nonlinear solutions to the equations are derived here for the general case $C_p \ne 0$ and for $C_p = 0$.

3.1.1. Solutions with $C_p \ne 0$: miscible mixing

For Rayleigh–Taylor mixing, $\Delta v = 0$. Substituting Eq. (51), the momentum equation (44) with $\overline{\nu} = 0$ becomes

$$\begin{aligned} \frac{d^2 h}{dt^2} = {} & C_b^*\, A t\, g_0 \left(\frac{t}{t_0}\right)^{\theta_{RT} - 2} \sqrt{\frac{C_p\, A t_\phi^2}{C_\chi} + \left(\Theta_0^2 - \frac{C_p\, A t_\phi^2}{C_\chi}\right)\left[\frac{h_0}{h(t)}\right]^{2C_\chi}} \\ & - \frac{C_d^*}{h}\left(\frac{dh}{dt}\right)^2 \,. \end{aligned} \tag{70}$$

Early-time solutions. At very early times, when $h_0/h \gg 1$, Eq. (70) reduces to

$$\frac{d^2h}{dt^2} \approx C_b^* A t g_0 \left(\frac{t}{t_0}\right)^{\theta_{RT}-2} \sqrt{\Theta_0^2 - \frac{C_p A t_\phi^2}{C_\chi}} \left(\frac{h_0}{h}\right)^{C_\chi} - \frac{C_d^*}{h}\left(\frac{dh}{dt}\right)^2 , \tag{71}$$

and Eq. (69) with $\overline{\nu} = 0$ reduces to

$$\theta_h\,(\theta_h - 1)\,A_h\,t^{\theta_h-2} = C_b^* A t g_0\, t_0^{2-\theta_{RT}} \sqrt{\Theta_0^2 - \frac{C_p A t_\phi^2}{C_\chi}} \left(\frac{h_0}{A_h}\right)^{C_\chi} t^{\theta_{RT}-2-\theta_h C_\chi} - C_d^* \theta_h^2 A_h\, t^{\theta_h-2} , \tag{72}$$

which requires $\theta_h - 2 = \theta_{RT} - 2 - \theta_h C_\chi$, or

$$\theta_h(C_\chi) = \frac{\theta_{RT}}{1 + C_\chi} ,$$

which decreases with increasing C_χ [and $\theta_h(0) = \theta_{RT}$, as required]. Therefore,

$$\theta_h\,(\theta_h - 1)\,A_h = C_b^* A t g_0\, t_0^{2-\theta_{RT}} \sqrt{\Theta_0^2 - \frac{C_p A t_\phi^2}{C_\chi}} \left(\frac{h_0}{A_h}\right)^{C_\chi} - C_d^* \theta_h^2 A_h ,$$

or

$$A_h(C_b^*, C_d^*, C_p, C_\chi; h_0, \Theta_0)$$

$$= \left[\frac{C_b^*\left(1 + C_\chi\right)^2 A t g_0\, t_0^{2-\theta_{RT}}\, h_0^{C_\chi}}{\theta_{RT}\left(\theta_{RT} + \theta_{RT}\, C_d^* - C_\chi - 1\right)} \sqrt{\Theta_0^2 - \frac{C_p A t_\phi^2}{C_\chi}}\right]^{1/(1+C_\chi)} ,$$

so that the analytic early-time power-law solution is

$$h(t) = \left[\frac{C_b^*\left(1 + C_\chi\right)^2 A t g_0\, t_0^{2-\theta_{RT}}\, h_0^{C_\chi}}{\theta_{RT}\left(\theta_{RT} + \theta_{RT}\, C_d^* - C_\chi - 1\right)}\right]^{1/(1+C_\chi)} \times \left[\Theta_0^2 - A t_\phi^2\,(1 - \theta_{mol})\right]^{1/[2(1+C_\chi)]}\, t^{\theta_{RT}/(1+C_\chi)} , \tag{73}$$

which depends on h_0 and Θ_0. This shows that $h(t)$ grows at early times with an exponent depending on the scalar variance dissipation rate coefficient C_χ, $\theta_{RT}/(1 + C_\chi) < \theta_{RT}$ for $C_\chi > 0$, i.e., grows slower than $t^{\theta_{RT}}$.

Late-time solutions. For late times, when $h_0/h \ll 1$, Eq. (70) simplifies to

$$\frac{d^2h}{dt^2} \approx C_b^* A t_\phi A t g_0 \sqrt{\frac{C_p}{C_\chi}} \left(\frac{t}{t_0}\right)^{\theta_{RT}-2} - \frac{C_d^*}{h}\left(\frac{dh}{dt}\right)^2 \tag{74}$$

and Eq. (69) with $\overline{\nu} = 0$ reduces to

$$\theta_h\,(\theta_h - 1)\,A_h\,t^{\theta_h-2} = C_b^* A t_\phi A t g_0 \sqrt{\frac{C_p}{C_\chi}} \left(\frac{t}{t_0}\right)^{\theta_{RT}-2} - C_d^* \theta_h^2 A_h\, t^{\theta_h-2} ,$$

which requires $\theta_h = \theta_{RT}$:

$$\theta_{RT}\,(\theta_{RT} - 1)\,A_h = C_b^* A t_\phi A t g_0 \sqrt{\frac{C_p}{C_\chi}}\, t_0^{2-\theta_{RT}} - C_d^* \theta_{RT}^2 A_h ,$$

so that

$$A_h(C_b^*, C_d^*, C_p, C_\chi) = \frac{C_b^* A t_\phi A t g_0\, t_0^{2-\theta_{RT}}}{\theta_{RT}\left(\theta_{RT} + \theta_{RT}\, C_d^* - 1\right)} \sqrt{\frac{C_p}{C_\chi}} .$$

Therefore, the analytic late-time power-law solution is

$$h(t) = \frac{C_b^* A t_\phi A t g_0\, t_0^{2-\theta_{RT}} \sqrt{1 - \theta_{mol}}}{\theta_{RT}\left(\theta_{RT} + \theta_{RT}\, C_d^* - 1\right)}\, t^{\theta_{RT}} , \tag{75}$$

$$\Theta = A t_\phi \sqrt{\frac{C_p}{C_\chi}} = A t_\phi \sqrt{1 - \theta_{mol}} . \tag{76}$$

Here, h does not depend on the initial values h_0 or Θ_0.

The corresponding velocity, acceleration, and normalized scalar variance are

$$v(t) = \frac{dh}{dt} = \frac{C_b^* \sqrt{1 - \theta_{mol}}\, A t_\phi A t g_0\, t_0^{2-\theta_{RT}}}{\theta_{RT} + \theta_{RT}\, C_d^* - 1}\, t^{\theta_{RT}-1} , \tag{77}$$

$$a(t) = \frac{dv}{dt} = \frac{(\theta_{RT} - 1)\, C_b^* \sqrt{1 - \theta_{mol}}\, A t_\phi A t g_0\, t_0^{2-\theta_{RT}}}{\theta_{RT} + \theta_{RT}\, C_d^* - 1}\, t^{\theta_{RT}-2} , \tag{78}$$

$$\frac{S(t)}{\overline{\phi}^2} = \frac{C_p A t_\phi^2}{C_\chi} = A t_\phi^2\,(1 - \theta_{mol}) . \tag{79}$$

The scalar variance dissipation rate can be reconstructed using

$$\chi(t) = C_\chi \frac{v(t)\, S(t)}{h(t)} = C_\chi \frac{\theta_{RT}\, S(t)}{t} , \tag{80}$$

and is proportional to θ_{RT}.

The width (75) can be written in the form (15) with mixing layer growth parameter

$$\alpha(\theta_{mol}) = \frac{C_b^* A t_\phi \sqrt{1 - \theta_{mol}}}{\theta_{RT}\left(\theta_{RT} + \theta_{RT}\, C_d^* - 1\right)} = \sqrt{1 - \theta_{mol}}\, \alpha(0) , \tag{81}$$

which is consistent with the model proposed by Ramaprabhu and Andrews [31], but different from the model later derived by Gréa [32]. *Incorporation of an active scalar in the buoyancy production term results in a Rayleigh–Taylor growth parameter that depends on the molecular mixing parameter* θ_{mol}. For constant acceleration, $\theta_{RT} = 2$, Eq. (81) reduces to

$$\alpha(C_b^*, C_d^*, \theta_{mol}) = \frac{C_b^* A t_\phi \sqrt{1 - \theta_{mol}}}{2\left(1 + 2\, C_d^*\right)} , \tag{82}$$

and the solutions reduce to the classical Rayleigh–Taylor solution (18) with $\theta_{mol} = 0$ and $A t_\phi = 1$.

Solving Eq. (81) for θ_{mol} gives

$$\theta_{mol}(\alpha) = 1 - \left[\frac{\alpha\, \theta_{RT}\left(\theta_{RT} + \theta_{RT}\, C_d^* - 1\right)}{C_b^* A t_\phi}\right]^2 , \tag{83}$$

which decreases with increasing α, consistent with the trends seen in numerical simulations of Rayleigh–Taylor mixing with α increasing due to larger long-wavelength initial perturbation content [33]. For a constant acceleration, this expression simplifies to

$$\theta_{mol}(\alpha) = 1 - \left[\frac{2\,\alpha\left(1 + 2\, C_d^*\right)}{C_b^* A t_\phi}\right]^2 .$$

3.1.2. *Solutions with $C_p = 0$: fully atomic miscible mixing*

Early-time solutions. If $C_p = 0$, Eq. (70) with Eq. (55) becomes

$$\frac{d^2h}{dt^2} = C_b^* A t g_0 \left(\frac{t}{t_0}\right)^{\theta_{RT}-2} \Theta_0 \left(\frac{h}{h_0}\right)^{-C_\chi} - \frac{C_d^*}{h}\left(\frac{dh}{dt}\right)^2 , \tag{84}$$

and Eq. (69) with $\overline{\nu} = 0$ reduces to

$$\theta_h\,(\theta_h - 1)\,A_h\,t^{\theta_h-2} = C_b^*\,At\,g_0\left(\frac{t}{t_0}\right)^{\theta_{RT}-2}\Theta_0\left(\frac{h_0}{A_h}\right)^{C_\chi} t^{-\theta_h C_\chi} - C_d^*\,\theta_h^2\,A_h\,t^{\theta_h-2}\,.$$

Setting $C_p = 0$ in Eq. (73) gives

$$h(t) = \left[\frac{C_b^*\left(1+C_\chi\right)^2\,At\,g_0\,t_0^{2-\theta_{RT}}\,\Theta_0\,h_0^{C_\chi}}{\theta_{RT}\left(\theta_{RT}+\theta_{RT}\,C_d^*-C_\chi-1\right)}\right]^{1/(1+C_\chi)} t^{\theta_{RT}/(1+C_\chi)}\,, \tag{85}$$

$$\Theta(t) = \Theta_0\left[\frac{h(t)}{h_0}\right]^{-C_\chi} = \Theta_0\left[\frac{C_b^*\left(1+C_\chi\right)^2\,At\,g_0\,t_0^{2-\theta_{RT}}\,\Theta_0}{\theta_{RT}\left(\theta_{RT}+\theta_{RT}\,C_d^*-C_\chi-1\right)h_0}\right]^{-C_\chi/(1+C_\chi)} t^{-\theta_{RT}C_\chi/(1+C_\chi)}\,. \tag{86}$$

With $C_\chi > 0$, the growth of $h(t)$ at early times is slower than $t^{\theta_{RT}}$. The corresponding velocity, acceleration, and normalized scalar variance are

$$v(t) = \frac{dh}{dt} = \frac{\theta_{RT}}{1+C_\chi}\left[\frac{C_b^*\left(1+C_\chi\right)^2\,At\,g_0\,t_0^{2-\theta_{RT}}\,\Theta_0\,h_0^{C_\chi}}{\theta_{RT}\left(\theta_{RT}+\theta_{RT}\,C_d^*-C_\chi-1\right)}\right]^{1/(1+C_\chi)} \times t^{(\theta_{RT}-1-C_\chi)/(1+C_\chi)}\,, \tag{87}$$

$$a(t) = \frac{dv}{dt} = \frac{\theta_{RT}\left(1-C_\chi\right)}{\left(1+C_\chi\right)^2} \times\left[\frac{C_b^*\left(1+C_\chi\right)^2\,At\,g_0\,t_0^{2-\theta_{RT}}\,\Theta_0\,h_0^{C_\chi}}{\theta_{RT}\left(\theta_{RT}+\theta_{RT}\,C_d^*-C_\chi-1\right)}\right]^{1/(1+C_\chi)} \times t^{(\theta_{RT}-2-2C_\chi)/(1+C_\chi)}\,, \tag{88}$$

$$\frac{S(t)}{\overline{\phi}^2} = \Theta(t)^2 = \Theta_0^2\left[\frac{C_b^*\left(1+C_\chi\right)^2\,At\,g_0\,t_0^{2-\theta_{RT}}\,\Theta_0}{\theta_{RT}\left(\theta_{RT}+\theta_{RT}\,C_d^*-C_\chi-1\right)h_0}\right]^{-2C_\chi/(1+C_\chi)} t^{-2\theta_{RT}C_\chi/(1+C_\chi)}\,. \tag{89}$$

The scalar variance dissipation rate can be reconstructed using

$$\chi(t) = C_\chi\frac{v(t)\,S(t)}{h(t)} = \frac{C_\chi}{1+C_\chi}\,\frac{\theta_{RT}\,S(t)}{t}\,. \tag{90}$$

The solutions depend on the initial values h_0 and Θ_0; they reduce to the classical (purely mechanical) Rayleigh–Taylor solution for $C_\chi = 0$ and $\theta_{RT} = 2$.

The mixing layer width (85) can be written as a modification to the classical form given by Eq. (15) with the time-dependent mixing layer growth parameter

$$\alpha(t) = \frac{1}{At}\left[\frac{C_b^*\left(1+C_\chi\right)^2\,At\,\Theta_0}{\theta_{RT}\left(\theta_{RT}+\theta_{RT}\,C_d^*-C_\chi-1\right)}\right]^{1/(1+C_\chi)}\left(\frac{h_0}{At\,g_0\,t_0^2}\right)^{C_\chi/(1+C_\chi)} \times\left(\frac{t}{t_0}\right)^{-\theta_{RT}C_\chi/(1+C_\chi)}\,, \tag{91}$$

which decreases in time at early times if $C_\chi > 0$ and is a function of g_0, At, h_0, Θ_0, C_b^*, C_d^*, and C_χ. For $C_\chi = 0$ and $\Theta_0 = 1$, Eq. (91) reduces to Eq. (18) as required.

Late-time solutions. At late times and taking $C_p = 0$ in Eq. (74) gives

$$\frac{d^2h}{dt^2} = -\frac{C_d^*}{h}\left(\frac{dh}{dt}\right)^2\,, \tag{92}$$

and Eq. (69) with $\overline{\nu} = 0$ reduces to

$$\theta_h\,(\theta_h - 1)\,A_h\,t^{\theta_h-2} = -C_d^*\,\theta_h^2\,A_h\,t^{\theta_h-2}\,,$$

which requires $\theta_h = 1/(1+C_d^*)$ but does not constrain A_h. The only dimensionally consistent solution is a power-law of the form (similar to Richtmyer–Meshkov instability)

$$h(t) = h_0\left(\frac{t}{t_0}\right)^{1/(1+C_d^*)}\,, \tag{93}$$

$$\Theta(t) = \Theta_0\left(\frac{t}{t_0}\right)^{-C_\chi/(1+C_d^*)}\,. \tag{94}$$

As $C_d^* > 0$, the power-law exponent for $h(t)$ is less than one.

The corresponding velocity, acceleration, and normalized scalar variance are

$$v(t) = \frac{dh}{dt} = \frac{h_0}{\left(1+C_d^*\right)t_0^{1/(1+C_d^*)}}\,t^{-C_d^*/(1+C_d^*)}\,, \tag{95}$$

$$a(t) = \frac{dv}{dt} = -\frac{C_d^*\,h_0}{\left(1+C_d^*\right)^2 t_0^{1/(1+C_d^*)}}\,t^{-(2C_d^*+1)/(1+C_d^*)}\,, \tag{96}$$

$$\frac{S(t)}{\overline{\phi}^2} = \Theta(t)^2 = \Theta_0^2\left(\frac{t}{t_0}\right)^{-2C_\chi/(1+C_d^*)}\,. \tag{97}$$

The solutions depend on the initial values h_0 and Θ_0. The scalar variance dissipation rate can be reconstructed using

$$\chi(t) = C_\chi\frac{v(t)\,S(t)}{h(t)} = \frac{C_\chi}{1+C_d^*}\,\frac{S(t)}{t}\,. \tag{98}$$

3.1.3. Solutions with $C_p = C_\chi$: immiscible mixing

Early-time solutions. Setting $C_p = C_\chi$ so that $\theta_{mol} = 0$ in Eq. (73) gives

$$h(t) = \left[\frac{C_b^*\left(1+C_\chi\right)^2\,At\,g_0\,t_0^{2-\theta_{RT}}\,h_0^{C_\chi}}{\theta_{RT}\left(\theta_{RT}+\theta_{RT}\,C_d^*-C_\chi-1\right)}\sqrt{\Theta_0^2 - At_\phi^2}\right]^{1/(1+C_\chi)} t^{\theta_{RT}/(1+C_\chi)}\,. \tag{99}$$

For the constant acceleration case with $\theta_{RT} = 2$, this becomes

$$h(t) = \left[\frac{C_b^*\left(1+C_\chi\right)^2\,At\,g_0\,h_0^{C_\chi}}{2\left(1+2\,C_d^*-C_\chi\right)}\sqrt{\Theta_0^2 - At_\phi^2}\right]^{1/(1+C_\chi)} t^{2/(1+C_\chi)}\,. \tag{100}$$

Again, the solutions depend on h_0 and Θ_0.

Late-time solutions. Setting $C_p = C_\chi$ so that $\theta_{mol} = 0$ in Eq. (75) gives

$$h(t) = \frac{C_b^*\,At_\phi\,At\,g_0\,t_0^{2-\theta_{RT}}}{\theta_{RT}\left(\theta_{RT}+\theta_{RT}\,C_d^*-1\right)}\,t^{\theta_{RT}} \tag{101}$$

with $\Theta = At_\phi$. For the constant acceleration case with $\theta_{RT} = 2$ and $At_\phi = 1$, this reduces to the classical width

$$h(t) = \frac{C_b^*}{2\left(1+2\,C_d^*\right)}\,At\,g_0\,t^2\,. \tag{102}$$

3.2. Richtmyer–Meshkov mixing

Analytic solutions to the equations are derived here for the general case $C_p \neq 0$ and for $C_p = 0$. Note that, unlike in the Rayleigh–Taylor case, the scalar is not actively coupled to the buoyancy–shear–drag equation because of the absence of a production term, so that $h(t)$ is independent of the degree of molecular mixing.

3.2.1. Solutions with $C_p \neq 0$: miscible mixing

For Richtmyer–Meshkov mixing, $\Delta v = 0$, Eq. (84) reduces to Eq. (92), and the scalar is passive. The analytic late-time mixing layer width is (16) with mixing layer growth exponent $\theta(C_d^*) = 1/\left(1 + C_d^*\right)$. The formal solution of Eq. (48) with $\Theta(t_0) = \Theta_0$ and $\overline{D} = 0$ is (51). The analytic power-law solution is

$$\Theta(t) = \sqrt{\frac{C_p\, At_\phi^2}{C_\chi} + \left(\Theta_0^2 - \frac{C_p\, At_\phi^2}{C_\chi}\right)\left(\frac{\Delta v_s\, At^+\, t}{\theta\, h_0}\right)^{-2\theta C_\chi}}\,, \tag{103}$$

which depends on both h_0 and Θ_0. The corresponding velocity, acceleration, and normalized scalar variance are

$$v(t) = \frac{dh}{dt} = \Delta v_s\, At^+ \left(\frac{\Delta v_s\, At^+\, t}{\theta\, h_0}\right)^{\theta-1}\,, \tag{104}$$

$$a(t) = \frac{dv}{dt} = \frac{\theta - 1}{\theta\, h_0}\left(\Delta v_s\, At^+\right)^2 \left(\frac{\Delta v_s\, At^+\, t}{\theta\, h_0}\right)^{\theta-1}\,, \tag{105}$$

$$\frac{S(t)}{\overline{\phi}^2} = \frac{C_p\, At_\phi^2}{C_\chi} + \left(\Theta_0^2 - \frac{C_p\, At_\phi^2}{C_\chi}\right)\left(\frac{\Delta v_s\, At^+\, t}{\theta\, h_0}\right)^{-2\theta C_\chi}\,. \tag{106}$$

These solutions decay in time. The scalar variance dissipation rate can be reconstructed using

$$\chi(t) = C_\chi \frac{v(t)\, S(t)}{h(t)} = C_\chi \frac{\theta\, S(t)}{t}\,. \tag{107}$$

3.2.2. Solutions with $C_p = 0$: fully-atomic miscible mixing

Taking $C_p = 0$ in the equations above gives

$$\Theta(t) = \Theta_0 \left(\frac{\Delta v_s\, At^+\, t}{\theta\, h_0}\right)^{-C_\chi \theta}\,, \tag{108}$$

$$\frac{S(t)}{\overline{\phi}^2} = \Theta_0^2 \left(\frac{\Delta v_s\, At^+\, t}{\theta\, h_0}\right)^{-2\theta C_\chi}\,, \tag{109}$$

which decay in time, approaching zero asymptotically. The solutions reduce to the classical Richtmyer–Meshkov solutions $\Theta(t) = \Theta_0$ and $S/\overline{\phi}^2 = \Theta_0^2$ for $C_\chi = 0$ for which $S = constant$ ($dS/dt = 0$).

3.2.3. Solutions with $C_p = C_\chi$: immiscible mixing

Taking $C_p = C_\chi$ in the equations above gives

$$\Theta(t) = \sqrt{At_\phi^2 + \left(\Theta_0^2 - At_\phi^2\right)\left(\frac{\Delta v_s\, At^+\, t}{\theta\, h_0}\right)^{-2\theta C_\chi}}\,, \tag{110}$$

$$\frac{S(t)}{\overline{\phi}^2} = At_\phi^2 + \left(\Theta_0^2 - At_\phi^2\right)\left(\frac{\Delta v_s\, At^+\, t}{\theta\, h_0}\right)^{-2\theta C_\chi}\,. \tag{111}$$

At late times, the solutions approach $\Theta = At_\phi$ and $S/\overline{\phi}^2 = At_\phi^2$.

3.3. Kelvin–Helmholtz mixing

Analytic solutions to the equations are derived here for the general case $C_p \neq 0$ and for $C_p = 0$.

3.3.1. Solutions with $C_p \neq 0$: miscible mixing

For Kelvin–Helmholtz mixing, $g_{\text{eff}} = 0$ and with the substitution (51), Eq. (44) reduces to

$$\frac{d^2h}{dt^2} = C_s^* \left\{1 - \frac{C_p\, At_\phi^2\, At^2}{C_\chi} - At^2\left(\Theta_0^2 - \frac{C_p\, At_\phi^2}{C_\chi}\right)\left[\frac{h_0}{h(t)}\right]^{2C_\chi}\right\}\frac{(\Delta v)^2}{h(t)} - C_d^*\,\frac{|v(t)\,\Delta v|}{h(t)} - \overline{\nu}\,\frac{v(t)}{h(t)^2}\,, \tag{112}$$

and Eq. (69) with $\overline{\nu} = 0$ reduces to

$$\theta_h\,(\theta_h - 1)\,A_h\, t^{\theta_h - 2}$$

$$= C_s^* \left[1 - \frac{C_p\, At_\phi^2\, At^2}{C_\chi} - At^2\left(\Theta_0^2 - \frac{C_p\, At_\phi^2}{C_\chi}\right)\left(\frac{h_0}{A_h}\right)^{2C_\chi} t^{-2\theta_h C_\chi}\right]\frac{(\Delta v)^2}{A_h}\, t^{-\theta_h} - C_d^*\,\frac{|\theta_h\,\Delta v|}{t}\,,$$

so that neglecting the small term proportional to $t^{-2\theta_h C_\chi}$ at late times requires $\theta_h - 2 = -\theta_h = -1$, or

$$\theta_h = 1\,, \tag{113}$$

$$\Theta(t) = \Theta_0 = At_\phi\sqrt{1 - \theta_{mol}}\,.$$

Therefore,

$$0 = C_s^*\left(1 - At^2\,\Theta_0^2\right)\frac{|\Delta v|}{A_h} - C_d^*\,,$$

or

$$A_h(C_s^*, C_d^*, \theta_{mol}) = \frac{C_s^*}{C_d^*}\left[1 - At^2\, At_\phi^2\,(1 - \theta_{mol})\right]|\Delta v|\,.$$

The analytic power-law solution for the mixing layer width is (17) with mixing layer growth parameter

$$\delta(C_s^*, C_d^*, \theta_{mol}) = \frac{C_s^*}{C_d^*}\left[1 - At^2\, At_\phi^2\,(1 - \theta_{mol})\right], \tag{114}$$

which depends on the ratio C_s^*/C_d^* and on θ_{mol}. The corresponding velocity, acceleration, and normalized scalar variance are

$$v(t) = \delta\,|\Delta v|\,, \tag{115}$$

$$a(t) = \frac{dv}{dt} = 0\,, \tag{116}$$

$$\frac{S(t)}{\overline{\phi}^2} = At_\phi^2\,(1 - \theta_{mol})\,. \tag{117}$$

The scalar variance dissipation rate can be reconstructed using

$$\chi(t) = C_\chi \frac{v(t)\, S(t)}{h(t)} = C_\chi \frac{S(t)}{t}\,. \tag{118}$$

Therefore, the solutions reduce to the classical Kelvin–Helmholtz solution when $\theta_{mol} = 0$ and $At_\phi = 1$. There is no dependence on θ_{mol} if $At = 0$, corresponding to Kelvin–Helmholtz mixing in a pure fluid, in which case the scalar is passive. If a nonpower-law solution with $C_\chi \neq 0$ can be found, then $S(t)$ will depend on time.

3.3.2. Solutions with $C_p = 0$: fully-atomic miscible mixing

If $C_p = 0$, Eq. (44) with Eq. (55) becomes

$$\frac{d^2h}{dt^2} = C_s^*\left\{1 - At^2\,\Theta_0^2\left[\frac{h_0}{h(t)}\right]^{2C_\chi}\right\}\frac{(\Delta v)^2}{h(t)} - C_d^*\,\frac{|v(t)\,\Delta v|}{h(t)} - \overline{\nu}\,\frac{v(t)}{h(t)^2}\,, \tag{119}$$

and Eq. (69) with $\overline{v} = 0$ reduces to

$$\theta_h\,(\theta_h - 1)\,A_h\,t^{\theta_h - 2} = C_s^*\left[1 - At^2\,\Theta_0^2\left(\frac{h_0}{A_h}\right)^{2C_\chi}\,t^{-2\theta_h C_\chi}\right]\frac{(\Delta v)^2}{A_h}\,t^{-\theta_h} - C_d^*\,\frac{|\theta_h\,\Delta v|}{t}\,,$$

so that neglecting the small term proportional to $t^{-2\theta_h C_\chi}$ at late times requires $\theta_h - 2 = -\theta_h = -1$, or

$$\theta_h = 1\,, \tag{120}$$

$$\Theta(t) = \Theta_0 = 0\,.$$

Therefore,

$$0 = C_s^*\,\frac{|\Delta v|}{A_h} - C_d^*\,,$$

or

$$A_h(C_s^*, C_d^*) = \frac{C_s^*}{C_d^*}\,|\Delta v|\,.$$

The analytic power-law solution for the mixing layer width is Eq. (17) with mixing layer growth parameter

$$\delta(C_s^*, C_d^*) = \frac{C_s^*}{C_d^*}\,. \tag{121}$$

The corresponding velocity and acceleration are the same as for the case with $C_p \neq 0$, and the normalized scalar variance is

$$\frac{S(t)}{\overline{\phi}^2} = 0\,.$$

In this case, the scalar variance dissipation rate is zero. These solutions also directly follow from the expressions derived for $C_p \neq 0$ by taking $At = 0$.

3.3.3. *Solutions with $C_p = C_\chi$: immiscible mixing*

Setting $\theta_{mol} = 0$ in Eq. (114) gives

$$\delta(C_s^*, C_d^*; At) = \frac{C_s^*}{C_d^*}\left(1 - At^2\,At_\phi^2\right), \tag{122}$$

$$\frac{S(t)}{\overline{\phi}^2} = At_\phi^2\,. \tag{123}$$

4. Calibration of the scalar variance dissipation coefficient C_χ in the total mixing layer width formulation

The calibration of the scalar variance dissipation coefficient C_χ is analogous to that used for the turbulence models discussed in Ref. [7].

Consider decaying isotropic turbulence described by Eq. (27) with $C_p = \overline{D} = 0$, Eq. (29), Eq. (31), and $\ell = h$:

$$\frac{dS}{dt} = -\,2\,C_\chi\,\frac{v(t)\,S(t)}{h(t)} = -2\,C_\chi\,\frac{d\ln h}{dt}\,S(t) = -\,2\,C_\chi\,\theta_h\,\frac{S(t)}{t}\,, \tag{124}$$

which depends on θ_h. Substituting the temporal power-law $S(t) = S_0\,(t/t_0)^{-n_s}$ into this equation gives the linear relationship between the decay exponent n_s and C_χ,

$$n_s(C_\chi) = 2\,C_\chi\,\theta_h\,. \tag{125}$$

The equation for the turbulent kinetic energy ($K = v^2/2$) in the absence of any instability production is obtained by first taking $g_{\rm eff} = \Delta v = \overline{v} = v_a = 0$, and $R_i = 1$ in Eq. (9):

$$\frac{dv}{dt} = -C_\epsilon\,\frac{v(t)^2}{h(t)}\,, \tag{126}$$

where the drag coefficient C_d^* has been replaced by the dissipation rate coefficient C_ϵ appropriate for decaying turbulence. Multiplying this equation by $v(t)$ then gives the turbulent kinetic energy equation (using $h = v\,t/\theta_h$)

$$\frac{dK}{dt} = -C_\epsilon\,\frac{v(t)^3}{h(t)} = -2\,\theta_h\,C_\epsilon\,\frac{K(t)}{t}\,, \tag{127}$$

which depends on θ_h. The turbulent kinetic energy decay exponent, n, is determined by substituting the temporal power-law $K(t) = K_0\,(t/t_0)^{-n}$ into Eq. (127) or

$$n(C_\epsilon) = 2\,\theta_h\,C_\epsilon \Longleftrightarrow C_\epsilon(n) = \frac{n}{2\,\theta_h}\,.$$

With the relationship between the scalar decay exponent and the turbulent kinetic energy decay exponent [see Eq. (B24) in Ref. [7]]

$$n_s(C_\chi) = \frac{3\,(2-n)}{2} = 2\,C_\chi\,\theta_h\,, \tag{128}$$

it follows that

$$C_\chi(C_\epsilon) = \frac{3\,(1 - \theta_h\,C_\epsilon)}{2\,\theta_h} \quad \text{or} \quad C_\chi(n) = \frac{3\,(2-n)}{4\,\theta_h}\,. \tag{129}$$

For $C_\chi > 0$, $\theta_h C_\epsilon < 1$ and $n < 2$. The value of C_χ depends on θ_h, so that it is different for each instability:

$$C_{\chi,RT}(\theta_{RT}, n) = \frac{3\,(2-n)}{4\,\theta_{RT}}\quad,\quad C_{\chi,RM}(\theta, n) = \frac{3\,(2-n)}{4\,\theta}\,, \tag{130}$$

$$C_{\chi,KH}(n) = \frac{3\,(2-n)}{4}\,.$$

However, in applications of Reynolds-averaged models with a scalar variance description, such as the K–L–a–V model [5], the decay timescale in the K and V equations $L/\sqrt{2K}$ (where K, L, and V are the turbulent kinetic energy, turbulent lengthscale, and scalar variance, respectively) is independent of the instabilities, so the decay exponents are universal. The analog of this in the present model would be to assume $\theta_h = 1$, in which case the *single* calibrated value is

$$C_\chi(C_\epsilon) = \frac{3\,(1 - C_\epsilon)}{2} \quad \text{or} \quad C_\chi(n) = \frac{3\,(2-n)}{4} \tag{131}$$

for all three instabilities, the value of which is uniquely determined by the choice of the value of n.

For example, with the decay exponent $n = 1.1$ [see the discussion of Eq. (139) in Ref. [7]], and $\theta_{mol} = 0.8$ for Rayleigh–Taylor, Richtmyer–Meshkov, and Kelvin–Helmholtz mixing,

$$C_\chi = 0.675\quad,\quad C_p = 0.135 \tag{132}$$

such that $C_p/C_\chi = 0.2$.

5. Analytic solutions of the general buoyancy–shear–drag–scalar model equations

To develop the analytic solutions of the general buoyancy–shear–drag–scalar model corresponding to bubbles and spikes, Eq. (1) with the buoyancy and shear forces (2) and (3) modified by taking (with $\ell = h$)

$$F_b^{3-i}(t) = C_b\,(\rho_1 - \rho_2)\,g_{\rm eff}(t)\,\Theta(t)\,, \tag{133}$$

$$F_s^{3-i}(t) = C_s\,\rho_i\,\frac{1 - At^2\,\Theta(t)^2}{4}\,\frac{(\Delta v)^2}{h_{3-i}(t)} \tag{134}$$

with the other forces unchanged gives

$$\begin{aligned}(\rho_{3-i} + C_{vm}^*\,\rho_i)\,\frac{d^2 h_{3-i}}{dt^2} &= C_b\,(\rho_1 - \rho_2)\,g_{\text{eff}}(t)\,\Theta(t) \\ &+ \frac{C_s}{4}\,\rho_i\left[1 - At^2\,\Theta(t)^2\right]\frac{(\Delta v)^2}{h_{3-i}(t)} \\ &- \frac{C_d}{b}\,\frac{\rho_i\,|v_{3-i}(t)|}{h_{3-i}(t)}\sqrt{[R_i\,v_{3-i}(t)]^2 + (\Delta v)^2} \\ &- C_a\,\frac{\rho_i\,v_a\,|v_{3-i}(t)|}{h_{3-i}(t)}\,.\end{aligned} \tag{135}$$

Analytical self-similar solutions of this equation can be obtained for the asymptotically constant value of $\Theta(t)$ given by Eq. (53).

5.1. Solutions for Rayleigh–Taylor, Richtmyer–Meshkov, and Kelvin–Helmholtz mixing

Substituting the generic bubble and spike mixing layer width

$$h_{3-i}(t) = A_{h,3-i}\,t^{\theta_{h,3-i}}\,, \tag{136}$$

where the constant coefficients $A_{h,3-i}$ and exponents $\theta_{h,3-i}$ are specific to each instability, into Eq. (135) and using Eqs. (53) and (59) gives

$$\begin{aligned}\mathcal{L}(t) &= C_b\,(\rho_1 - \rho_2)\,g_{\text{eff}}(t)\,At_\phi\,\sqrt{1 - \theta_{mol,RT}} \\ &+ \frac{C_s}{4}\,\rho_i\left[1 - At^2\,At_\phi^2\,(1 - \theta_{mol,KH})\right]\frac{(\Delta v)^2}{A_{h,3-i}\,t^{\theta_{h,3-i}}} \\ &- \frac{C_d}{b}\,\frac{\rho_i\,\theta_{h,3-i}}{t}\sqrt{(R_i\,\theta_{h,3-i}\,A_{h,3-i}\,t^{\theta_{h,3-i}-1})^2 + (\Delta v)^2} \\ &- C_a\,\frac{\rho_i\,v_a\,\theta_{h,3-i}}{t}\end{aligned} \tag{137}$$

with $\mathcal{L}(t) = \theta_{h,3-i}\,(\theta_{h,3-i} - 1)(\rho_{3-i} + C_{vm}^*\rho_i)\,A_{h,3-i}t^{\theta_{h,3-i}-2}$.

For Rayleigh–Taylor ($\Delta v = v_a = 0$), Richtmyer–Meshkov ($g_0 = \Delta v = v_a = 0$), and Kelvin–Helmholtz ($g_{\text{eff}} = R_i = v_a = 0$) instability, the coefficients in the mixing layer widths and exponents are

$$A_{h,3-i} = \alpha_{3-i}\,At_\phi\,At\,g_0\,t_0^{2-\theta_{RT}}\quad,\quad \theta_{h,3-i} = \theta_{RT}\,, \tag{138}$$

$$A_{h,3-i} = h_{0,3-i}\left(\frac{\Delta v_s\,At^+}{\theta_{3-i}\,h_{0,3-i}}\right)^{\theta_{3-i}}\quad,\quad \theta_{h,3-i} = \theta_{3-i}\,, \tag{139}$$

$$A_{h,3-i} = \delta_{3-i}\,|\Delta v|\quad,\quad \theta_{h,3-i} = 1\,, \tag{140}$$

respectively. With these substitutions, Eq. (137) reduces to

$$\begin{aligned}\theta_{RT}\,(\theta_{RT} - 1)\,(\rho_{3-i} + C_{vm}^*\,\rho_i)\,\alpha_{3-i} &= C_b\,(\rho_1 - \rho_2)\,\sqrt{1 - \theta_{mol,RT}} \\ &- \frac{C_d}{b}\,\theta_{RT}^2\,\rho_i\,R_i\,\alpha_{3-i}\,, \\ (\theta_{3-i} - 1)\,(\rho_{3-i} + C_{vm}^*\,\rho_i) &= -\frac{C_d}{b}\,\theta_{3-i}\,\rho_i\,R_i\,, \\ 0 &= \frac{C_s}{4}\left[1 - At^2\,At_\phi^2\,(1 - \theta_{mol,KH})\right]\frac{1}{\delta_{3-i}} - \frac{C_d}{b}\end{aligned}$$

for each instability, and solving for α_{3-i}, θ_{3-i}, and δ_{3-i} gives

$$\alpha_{3-i}(C_b, C_d, C_{vm}^*, \theta_{mol,RT}) \tag{141}$$

$$= \frac{C_b\,(\rho_{3-i} + \rho_i)\,At_\phi\,\sqrt{1 - \theta_{mol,RT}}}{\theta_{RT}\,(\theta_{RT} - 1)(\rho_{3-i} + C_{vm}^*\,\rho_i) + \frac{\theta_{RT}^2\,C_d}{b}\,\rho_i\,R_i}\,,$$

$$\theta_{3-i}(C_d, C_{vm}^*) = \frac{\rho_{3-i} + C_{vm}^*\,\rho_i}{\rho_{3-i} + \left(C_{vm}^* + \frac{C_d}{b}\,R_i\right)\rho_i}, \tag{142}$$

$$\delta_{3-i}(C_s, C_d, \theta_{mol,KH}) = \frac{b\,C_s}{4\,C_d}\left[1 - At^2\,At_\phi^2\,(1 - \theta_{mol,KH})\right] \tag{143}$$

for the bubble and spike. It follows that the corresponding values for the total (bubble plus spike) mixing layer widths are

$$\begin{aligned}\alpha(\theta_{mol,RT}) &= \alpha_1 + \alpha_2 \\ &= \frac{C_b\,(\rho_1 + \rho_2)\,At_\phi\,\sqrt{1 - \theta_{mol,RT}}}{\theta_{RT}\,(\theta_{RT} - 1)(\rho_1 + C_{vm}^*\,\rho_2) + \frac{\theta_{RT}^2\,C_d}{b}\,\rho_2\,R_2} \\ &+ \frac{C_b\,(\rho_2 + \rho_1)\,At_\phi\,\sqrt{1 - \theta_{mol,RT}}}{\theta_{RT}\,(\theta_{RT} - 1)(\rho_2 + C_{vm}^*\,\rho_1) + \frac{\theta_{RT}^2\,C_d}{b}\,\rho_1\,R_1}\,,\end{aligned} \tag{144}$$

$$\delta(\theta_{mol,KH}) = \delta_1 + \delta_2 = \frac{b\,C_s}{2\,C_d}\left[1 - At^2\,At_\phi^2\,(1 - \theta_{mol,KH})\right]. \tag{145}$$

Note that the bubble and spike growth exponents for Richtmyer–Meshkov mixing are not additive. However, for very large times, $\theta \to \max(\theta_b, \theta_s)$. These expressions consistently reduce to the analogous expressions in Ref. [10] with $\theta_{mol,RT} = \theta_{mol,KH} = 0$ and $\theta_{RT} = 2$.

These analytic solutions confirm that the model equations are consistent with the expected temporal scalings of mixing [i.e., Eqs. (138)–(140)] induced by the instabilities. The solutions also provide relationships between growth parameters and exponents and the model coefficients (analogous to those obtained in self-similar analyses of Reynolds-averaged models [7–9]) that can be used to calibrate the model as a function of Atwood number.

The bubble and spike and total turbulent kinetic energy, turbulent kinetic energy dissipation rate, turbulent lengthscale, and Reynolds number are given by Eqs. (30)–(37) in Ref. [10].

5.2. Calibration of mechanical coefficients

The expressions for the growth parameters and exponent provide three equations for four coefficients C_b, C_{vm}^*, C_d, and C_s; a value of C_{vm}^* will be assumed later. Only the three-dimensional case is considered here, so that $b = 2/3$.

The calibration appropriate for finite Atwood number described above will be used here. With $R_i = 1$ and using $\rho_1/\rho_2 = (1 + At)/(1 - At)$, it follows that (choosing $\theta = \theta_s$)

$$\alpha(C_b, C_d, C_{vm}^*, \theta_{mol,RT}) \tag{146}$$

$$\begin{aligned}&= \frac{C_b\,(\rho_2 + \rho_1)\,At_\phi\,\sqrt{1 - \theta_{mol,RT}}}{\theta_{RT}\,(\theta_{RT} - 1)(\rho_1 + C_{vm}^*\,\rho_2) + \frac{\theta_{RT}^2\,C_d}{b}\,\rho_2} \\ &+ \frac{C_b\,(\rho_1 + \rho_2)\,At_\phi\,\sqrt{1 - \theta_{mol,RT}}}{\theta_{RT}\,(\theta_{RT} - 1)(\rho_2 + C_{vm}^*\,\rho_1) + \frac{\theta_{RT}^2\,C_d}{b}\,\rho_1} \\ &= \frac{2\,C_b\,At_\phi\,\sqrt{1 - \theta_{mol,RT}}}{\left[\theta_{RT}\,(\theta_{RT} - 1)\left(\frac{1+At}{1-At} + C_{vm}^*\right) + \frac{\theta_{RT}^2\,C_d}{b}\right](1 - At)} \\ &+ \frac{2\,C_b\,At_\phi\,\sqrt{1 - \theta_{mol,RT}}}{\left[\theta_{RT}\,(\theta_{RT} - 1)\left(\frac{1-At}{1+At} + C_{vm}^*\right) + \frac{\theta_{RT}^2\,C_d}{b}\right](1 + At)}\,,\end{aligned}$$

$$\theta(C_d, C^*_{vm}) = \frac{\rho_1 + C^*_{vm}\rho_2}{\rho_1 + \left(C^*_{vm} + \frac{C_d}{b}\right)\rho_2} = \frac{\frac{1+At}{1-At} + C^*_{vm}}{\frac{1+At}{1-At} + C^*_{vm} + \frac{C_d}{b}}\,, \tag{147}$$

$$\delta(C_s, C_d, \theta_{mol,KH}) = \frac{b\,C_s}{2\,C_d}\left[1 - At^2\,At_\phi^2\,(1-\theta_{mol,KH})\right], \tag{148}$$

each of which is a function of the Atwood number. Kelvin–Helmholtz growth decreases with increasing At. Solving these algebraic equations gives the analytic expressions for the buoyancy, shear, and drag coefficients ($At \neq 1$)

$$C_b(\alpha,\theta) = \frac{f(\alpha,\theta)}{g(\theta)}\,, \tag{149}$$

$$C_d(\theta) = \frac{b\,(1-\theta)[1 + C^*_{vm} + (1-C^*_{vm})\,At]}{\theta\,(1-At)}\,, \tag{150}$$

$$C_s(\delta,\theta) = \frac{2\,(1-\theta)[1 + C^*_{vm} + (1-C^*_{vm})\,At]\,\delta}{\theta\,(1-At)\left[1 - At^2\,At_\phi^2\,(1-\theta_{mol,KH})\right]} \tag{151}$$

with

$$\begin{aligned} f(\alpha,\theta) = {} & [1 + C^*_{vm} + (1-C^*_{vm})\,At]\,\alpha\,(\theta_{RT} - \theta)\,\theta_{RT} \\ & \times \{(1-At)[1 + C^*_{vm} + At\,(C^*_{vm} - 1)]\,\theta \\ & + [At\,(At\,C^*_{vm} - At + 4\,\theta - 2) - 1 - C^*_{vm}]\,\theta_{RT}\}\,, \end{aligned} \tag{152}$$

$$\begin{aligned} g(\theta) = {} & 4\,\theta\,At_\phi\,\sqrt{1-\theta_{mol,RT}} \\ & \times \{\theta_{RT}\,[At\,(C^*_{vm} + 2\,\theta - 1) - 1 - C^*_{vm}] + (1-At)\,(1 + C^*_{vm})\,\theta\}\,. \end{aligned} \tag{153}$$

For example, taking [7, 10, 34]

$$\alpha = 0.05 \;\;,\;\; \theta = 0.30 \;\;,\;\; \delta = 0.07 \tag{154}$$

for Rayleigh–Taylor, Richtmyer–Meshkov [35, 36], and Kelvin–Helmholtz mixing [37, 38], respectively, and $\theta_{mol,RT} = \theta_{mol,KH} = 0.8$ gives the coefficients

$$C_b(C^*_{vm}, At) = \frac{f(0.05, 0.3)}{g(0.3)}\,, \tag{155}$$

$$C_d(C^*_{vm}, At) = \frac{1.5556[1 + C^*_{vm} + (1-C^*_{vm})\,At]}{1-At}\,, \tag{156}$$

$$C_s(C^*_{vm}, At) = \frac{0.3267[1 + C^*_{vm} + (1-C^*_{vm})\,At]}{(1-At)\left(1 - 0.2\,At^2\,At_\phi^2\right)}\,. \tag{157}$$

6. Calibration of the general scalar variance dissipation coefficient C_χ

A procedure similar to that used in Section 4 generalized to bubbles and spikes can be used to calibrate the coefficient C_χ for each instability.

Consider decaying isotropic turbulence: the decaying scalar variance equation is the same as Eq. (124), together with Eq. (125). To derive the turbulent kinetic energy equation in the absence of any instabilities, first take $g_{\rm eff} = \Delta v = v_a = 0$ and $R_i = 1$ in Eq. (135):

$$(\rho_{3-i} + C^*_{vm}\rho_i)\,\frac{dv_{3-i}}{dt} = -\frac{C_d}{b}\,\frac{\rho_i\,v_{3-i}(t)^2}{h_{3-i}(t)}\,. \tag{158}$$

In an asymptotically fully-mixed decaying state, the densities reduce to the average density of the mixture $\rho_i \to (\rho_1 + \rho_2)/2$, and assuming that $h_{3-i} = h(t)/2$, these approximations simplify Eq. (158) to

$$\frac{d^2h}{dt^2} = -\frac{C_d}{b\,(1 + C^*_{vm})}\,\frac{1}{h(t)}\left(\frac{dh}{dt}\right)^2\,, \tag{159}$$

which has the same mathematical form as Eq. (92). Substituting the power-law $h(t) = h_0\,(t/t_0)^{n_h}$ into this equation gives the growth exponent

$$n_h(C_d, C^*_{vm}, b) = \frac{b\,(1 + C^*_{vm})}{b\,(1 + C^*_{vm}) + C_d}\,.$$

Therefore, the turbulent kinetic energy is

$$K(t) = \frac{v(t)^2}{2} = \frac{1}{2}\left(\frac{dh}{dt}\right)^2 = \frac{1}{2}\left(\frac{n_h\,h_0}{t_0}\right)^2\left(\frac{t}{t_0}\right)^{-n}$$

with decay exponent

$$n(C_d, C^*_{vm}, b) = -2\,(n_h - 1) = \frac{2\,C_d}{b\,(1 + C^*_{vm}) + C_d}\,. \tag{160}$$

With the relationship between the scalar decay exponent and the turbulent kinetic energy decay exponent (128) it follows that

$$C_\chi(C_d, C^*_{vm}, b) = \frac{3}{2\,\theta_h}\,\frac{b\,(1 + C^*_{vm})}{b\,(1 + C^*_{vm}) + C_d} \quad \text{or} \quad C_\chi(n) = \frac{3\,(2-n)}{4\,\theta_h}\,. \tag{161}$$

The value of C_χ depends on θ_h, so that it is different for each instability:

$$C_{\chi,RT}(\theta_{RT}, C_d, C^*_{vm}, b) = \frac{3}{2\,\theta_{RT}}\,\frac{b\,(1 + C^*_{vm})}{b\,(1 + C^*_{vm}) + C_d}\,, \tag{162}$$

$$C_{\chi,RM}(\theta, C_d, C^*_{vm}, b) = \frac{3}{2\,\theta}\,\frac{b\,(1 + C^*_{vm})}{b\,(1 + C^*_{vm}) + C_d}\,,$$

$$C_{\chi,KH}(C_d, C^*_{vm}, b) = \frac{3}{2}\,\frac{b\,(1 + C^*_{vm})}{b\,(1 + C^*_{vm}) + C_d}\,.$$

These expressions are equivalent to those in Eq. (130), but with n given by Eq. (160), and will subsequently be used in the applications discussed in Section 8. The scalar variance dissipation coefficient does not depend on the Atwood number.

7. The buoyancy–shear–drag–scalar turbulence model in the total mixing layer width formulation

The buoyancy–shear–drag–scalar model equations for the total mixing layer widths and scalar variance discussed above are given here for each instability case using the calibrations of the mechanical and scalar coefficients. Only the calibrated model coefficients and construction of the turbulent fields will be given; the equations are solved numerically for the bubbles and spikes separately in Section 8.

7.1. Model calibration using instability growth parameters and exponents, and scalar coefficients

The calibrations of the mechanical and scalar model coefficients for the passive and active scalar cases are given here.

7.1.1. Passive scalar mechanical coefficients

Substituting the values in Eq. (154) into Eqs. (20)–(22) gives the mechanical coefficients

$$C^*_b = 0.1667\,\theta_{RT}\,(\theta_{RT} - 0.3) \;\;,\;\; C^*_d = 2.3333 \;\;,\;\; C^*_s = \frac{0.1633}{1 - At^2}\,. \tag{163}$$

For $\theta_{RT} = 2$, $C^*_b = 0.5668$. For this particular choice, $C^*_b > 0$ requires $\theta_{RT} > 0.3$.

7.1.2. Active scalar mechanical coefficients

For the active scalar case, solving Eqs. (81), (19), and (114) for the buoyancy, drag, and shear coefficients gives

$$C^*_b(\alpha, \theta, \theta_{mol,RT}) = \frac{\alpha\,\theta_{RT}\,(\theta_{RT} - \theta)}{At_\phi\,\theta\,\sqrt{1 - \theta_{mol,RT}}} \;\;,\;\; C^*_d(\theta) = \frac{1-\theta}{\theta}\,, \tag{164}$$

$$C_s^*(\delta,\theta,\theta_{mol,KH}) = \frac{(1-\theta)\,\delta}{\theta\left[1 - At^2\,At_\phi^2\,(1-\theta_{mol,KH})\right]}\,,$$

which reduce to the passive expressions with $\theta_{mol,RT} = \theta_{mol,KH} = 0$ and $At_\phi = 1$, as required. For constant acceleration, $C_b^* = 2\alpha\,(2-\theta)\,/[At_\phi\theta\sqrt{1-\theta_{mol,RT}}]$.

Substituting the values in Eq. (154) into these equations gives the mechanical coefficients

$$C_b^* = \frac{0.1667\,\theta_{RT}\,(\theta_{RT}-0.3)}{At_\phi\sqrt{1-\theta_{mol,RT}}}\;,\; C_d^* = 2.3333\,, \tag{165}$$

$$C_s^* = \frac{0.1633}{1 - At_\phi^2\,At^2\,(1-\theta_{mol,KH})}\,.$$

For $\theta_{RT} = 2$, $C_b^* = 0.5668/[At_\phi\sqrt{1-\theta_{mol,RT}}]$.

7.1.3. Active and passive scalar coefficients

For example, with the decay exponent $n = 1.1$, $\theta = 0.3$, and $\theta_{mol} = 0.8$ for Rayleigh–Taylor, Richtmyer–Meshkov, and Kelvin–Helmholtz mixing, Eqs. (130) and (59) give the scalar coefficients

$$C_{\chi,RT} = \frac{0.675}{\theta_{RT}}\;\;,\;\; C_{p,RT} = \frac{0.135}{\theta_{RT}}\,, \tag{166}$$

$$C_{\chi,RM} = 2.25\;\;,\;\; C_{p,RM} = 0.45\,,$$

$$C_{\chi,KH} = 0.675\;\;,\;\; C_{p,KH} = 0.135\,,$$

respectively. For $\theta_{RT} = 2$, $C_{\chi,RT} = 0.3375$ and $C_{p,RT} = 0.0675$.

If the equations are solved numerically for combined instabilities, the value of C_χ could be chosen to be that corresponding to the dominant instability. Alternatively, a coefficient that blends the values and weights them according to, for example, a Richardson number could be used. The universal calibration (132) can also be used.

7.2. Construction of turbulent quantities

Turbulent quantities corresponding to the mixing layers can be constructed from h and $v = dh/dt$ as derived in a general form for the bubble and spike in Ref. [10]. The corresponding turbulent quantities were constructed in Ref. [10] as sums of bubble and spike quantities; here, they are given in the total mixing layer formulation for completeness.

7.2.1. Time-dependent quantities

The turbulent kinetic energy, turbulent kinetic dissipation rate, turbulent lengthscale, and turbulent mixing layer Reynolds number at late-time are

$$K(t) = \frac{v(t)^2}{2} = \frac{\theta_h^2\,A_h^2}{2}\,t^{2\theta_h-2}\,, \tag{167}$$

$$\begin{aligned}\epsilon(t) &= \frac{C_d^*}{2\rho_0}\,\frac{v(t)^2}{h(t)}\left[\rho_1\sqrt{\left[R_1^n\,v(t)\right]^2 + (\Delta v)^2} + \rho_2\sqrt{[R_2\,v(t)]^2 + (\Delta v)^2}\right] \\ &= \frac{C_d^*}{2\rho_0}\,\theta_h^2\,A_h \\ &\quad\times\left[\rho_1\sqrt{\left(R_1^n\,\theta_h\,A_h\,t^{\theta_h-1}\right)^2 + (\Delta v)^2} + \rho_2\sqrt{\left(R_2\,\theta_h\,A_h\,t^{\theta_h-1}\right)^2 + (\Delta v)^2}\right] \\ &\quad\times t^{\theta_h-2}\,,\end{aligned} \tag{168}$$

$$\begin{aligned}L(t) &= C_L\,\frac{K(t)^{3/2}}{\epsilon(t)} \\ &= \frac{C_L}{\sqrt{2}\,C_d^*}\,\theta_h\,A_h^2\,\rho_0 \\ &\quad\times\left[\rho_1\sqrt{\left(R_1^n\,\theta_h\,A_h\,t^{\theta_h-1}\right)^2 + (\Delta v)^2}\right. \\ &\quad\left.+\,\rho_2\sqrt{\left(R_2\,\theta_h\,A_h\,t^{\theta_h-1}\right)^2 + (\Delta v)^2}\right]^{-1} \\ &\quad\times t^{2\theta_h-1}\,,\end{aligned} \tag{169}$$

$$Re_h(t) = \frac{v(t)\,h(t)}{\bar\nu} = \frac{\theta_h\,A_h^2}{\bar\nu}\,t^{2\theta_h-1}\,. \tag{170}$$

The mechanical and scalar timescales are [7]

$$\begin{aligned}\tau_m(t) &= \frac{K(t)}{\epsilon(t)} \\ &= \frac{\rho_0}{C_d^*}\,h(t)\left[\rho_1\sqrt{\left[R_1^n\,v(t)\right]^2 + (\Delta v)^2} + \rho_2\sqrt{[R_2\,v(t)]^2 + (\Delta v)^2}\right]^{-1}\,,\end{aligned} \tag{171}$$

$$\tau_s(t) = \frac{S(t)}{2\chi(t)}$$

for the algebraic scalar variance dissipation rate Eq. (31), and the constant mechanical-to-scalar timescale ratio is

$$\begin{aligned}R &= \frac{\tau_m(t)}{\tau_s(t)} \\ &= \frac{2\,C_\chi\,\rho_0}{C_d^*}\,v(t)\left[\rho_1\sqrt{\left[R_1^n\,v(t)\right]^2 + (\Delta v)^2} + \rho_2\sqrt{[R_2\,v(t)]^2 + (\Delta v)^2}\right]^{-1}\,.\end{aligned} \tag{172}$$

For Rayleigh–Taylor mixing with the simplification $R_1 = R_2 = 1$, $\tau_m = h(t)/[2C_d^*v(t)]$ (differing by a factor of $1/(2C_d^*)$ from the definition in Section 2.1.2).

Using Eq. (10), a mixing layer turbulent diffusion coefficient is given dimensionally for each instability by the general expression

$$D_h(t) = C_D\,h\,\frac{dh}{dt} = C_D\,\theta_h\,A_h^2\,t^{2\theta_h-1}\,, \tag{173}$$

where C_D is a dimensionless coefficient. The corresponding mixing layer turbulent viscosity coefficient is $\nu_h(t) = Sc_t D_h(t)$, where Sc_t is the (constant) turbulent Schmidt number (typically assumed to be 0.7).

An alternative expression inspired by the K–ϵ model is

$$\begin{aligned}\nu_h(t) &= C_\nu\,\frac{K(t)^2}{\epsilon(t)} \\ &= \frac{C_\nu\,\theta_h^2\,A_h^3\,t^{3\theta_h-2}}{4\,C_d^*} \\ &\quad\times\left[\rho_1\sqrt{(R_1\,\theta_h\,A_h\,t^{\theta_h-1})^2 + (\Delta v)^2}\right. \\ &\quad\left.+\,\rho_2\sqrt{(R_2\,\theta_h\,A_h\,t^{\theta_h-1})^2 + (\Delta v)^2}\right]^{-1} \\ &= Sc_t\,D_h(t)\,.\end{aligned} \tag{174}$$

This expression could be used in applications with $C_\nu = 1$, $D_h \to D_t$, and $\nu_h \to \nu_t$.

In the expressions above that include the terms with R_i, $v(t)$ should either be independent of time (as it is in Kelvin–Helmholtz mixing) or be zero in order that these expressions have a single time dependence (as would be required by self-similarity).

7.2.2. Spatiotemporal quantities

As described in Ref. [10], a spatially-dependent turbulent diffusion coefficient across the mixing layer can be constructed as (z_{int} is the location of the initial interface separating the heavy and light fluids) a self-similar inverse parabolic, Gaussian, or product of an inverse parabolic and Gaussian profile,

$$D_t(z,t) = D_h(t)\,\frac{f\left(\frac{z-z_{int}}{h(t)}\right)}{\max\left[f\left(\frac{z-z_{int}}{h(t)}\right)\right]}\,, \tag{175}$$

where

$$f\left(\frac{z-z_{int}}{h(t)}\right) = 1 - \frac{(z-z_{int})^2}{h(t)^2}\,, \tag{176}$$

$$f\left(\frac{z-z_{int}}{h(t)}\right) = \exp\left[-\frac{4\,(z-z_{int})^2}{h(t)^2}\right], \tag{177}$$

$$f\left(\frac{z-z_{int}}{h(t)}\right) = \left[1 - \frac{(z-z_{int})^2}{h(t)^2}\right]\exp\left[-\frac{4\,(z-z_{int})^2}{h(t)^2}\right], \tag{178}$$

respectively. These expressions can be generalized to include h_b and h_s. Higher-order profiles generalizing the inverse parabolic profiles of the form

$$f\left(\frac{z-z_{int}}{h(t)}\right) = \left[1 - \frac{(z-z_{int})^2}{h(t)^2}\right]^{n_D} \tag{179}$$

with $n_D > 1$ similar to the form used in a Reynolds-averaged turbulence model [39] to fit late-time profiles obtained from numerical simulations and inspired by a previous analysis of a Reynolds-averaged model [40] could also be used. In this case, the turbulent fields would, in general, have different exponents $\{n_\phi\}$ chosen such that each resulting field profile closely matches the corresponding profile obtained from the simulations. In general, the spatial profiles are normalized by their maximum value and are required to be positive for realizability.

The corresponding turbulent viscosity is

$$\nu_t(z,t) = Sc_t\,D_t(z,t)\,. \tag{180}$$

7.2.3. Turbulent kinetic energy and turbulent kinetic energy dissipation rate equations

For reference, an equation for the turbulent kinetic energy $K(t) = v(t)^2/2$ follows by multiplying Eq. (44) by $v(t)$:

$$\begin{aligned}\frac{dK}{dt} &= C_b^*\,g_{\rm eff}(t)\,At\,\Theta(t)\,v(t) + C_s^*\left[1 - At^2\,\Theta(t)^2\right]\frac{(\Delta v)^2\,v(t)}{h(t)} \\ &\quad - \frac{C_d^*}{\rho_1+\rho_2}\,\frac{|v(t)|\,v(t)}{h(t)} \\ &\quad \times\left[\rho_1\sqrt{\left[R_1^n\,v(t)\right]^2 + (\Delta v)^2} + \rho_2\sqrt{[R_2\,v(t)]^2 + (\Delta v)^2}\right] \\ &\quad - 2\,\overline{\nu}\,\frac{K(t)}{h(t)^2} - 2\,C_a^*\,\frac{v_a\,K(t)}{h(t)}\,.\end{aligned} \tag{181}$$

An equation for the turbulent kinetic energy dissipation rate $\epsilon(t)$ follows by dividing the right side of Eq. (181) by the mechanical turbulent timescale $\tau_m = K/\epsilon = h/v$ and introducing a dimensionless coefficient $C_{\epsilon q}$ (in which numerical factors and the previous coefficients have been absorbed) in each term:

$$\begin{aligned}\frac{d\epsilon}{dt} &= C_{\epsilon 0}\,g_{\rm eff}(t)\,At\,\Theta(t)\,\frac{K(t)}{h(t)} + C_{\epsilon 1}\left[1 - At^2\,\Theta(t)^2\right]\frac{(\Delta v)^2\,K(t)}{h(t)^2} \\ &\quad - \frac{C_{\epsilon 2}}{\rho_1+\rho_2}\,\frac{|v(t)|\,K(t)}{h(t)^2} \\ &\quad \times\left[\rho_1\sqrt{\left[R_1^n\,v(t)\right]^2 + (\Delta v)^2} + \rho_2\sqrt{[R_2\,v(t)]^2 + (\Delta v)^2}\right] \\ &\quad - C_{\epsilon 4}\,\overline{\nu}\,\frac{K(t)^{3/2}}{h(t)^3} - C_{\epsilon 5}\,\frac{v_a\,K(t)^{3/2}}{h(t)^2}\,.\end{aligned} \tag{182}$$

The coefficients $\{C_{\epsilon q}\}$ can be calibrated using a procedure similar to what was used for the BSDS model, and would require the introduction of additional physical quantities (beyond α, θ, and δ) to determine the values of the coefficients in the ϵ equation (similar to the calibration of Reynolds-averaged models).

7.2.4. The closed mean flow equations

The gradient-diffusion closure of the one-dimensional, variable-density incompressible mean heavy mass fraction, mean momentum, and mean shear velocity equations, respectively, are given here for reference. These equations can be solved numerically using the expressions for the turbulent diffusivity and viscosity constructed above.

The mean heavy mass fraction equation is ($\widetilde{w} = \overline{\rho w}/\overline{\rho}$ is the mean velocity in the z-direction parallel to the acceleration)

$$\begin{aligned}\overline{\rho}\left(\frac{\partial}{\partial t} + \widetilde{w}\,\frac{\partial}{\partial z}\right)\widetilde{m}_H &= \frac{\partial}{\partial z}\left(\overline{\rho}\,\overline{D}\,\frac{\partial \widetilde{m}_H}{\partial z} - \overline{\rho\,m_H''\,w''}\right) \\ &= \frac{\partial}{\partial z}\left[\overline{\rho}\left(\overline{D} + D_t\right)\frac{\partial \widetilde{m}_H}{\partial z}\right]\end{aligned} \tag{183}$$

in the Fickian diffusion approximation (the mean light fluid mass fraction is $\widetilde{m}_L = 1 - \widetilde{m}_H$). The heavy and light fluids correspond to the spike and bubble, respectively. The mean momentum equation is (with mean kinematic molecular and turbulent kinematic viscosities $\overline{\mu} = \overline{\rho}\,\overline{\nu}$ and $\mu_t = \overline{\rho}\,\nu_t$)

$$\begin{aligned}\overline{\rho}\left(\frac{\partial}{\partial t} + \widetilde{w}\,\frac{\partial}{\partial z}\right)\widetilde{w} &= \overline{\rho}\,g_{\rm eff} - \frac{\partial \overline{p}}{\partial z} + \frac{\partial \overline{\sigma}_{zz}}{\partial z} - \frac{\partial \tau_{zz}}{\partial z} \\ &= \overline{\rho}\,g_{\rm eff} - \frac{\partial \overline{p}}{\partial z} + \frac{\partial}{\partial z}\left(2\,\overline{\mu}\,\frac{\partial \widetilde{w}}{\partial z}\right) \\ &\quad - \frac{\partial}{\partial z}\left(\frac{2}{3}\,\overline{\rho}\,K - 2\,\mu_t\,\frac{\partial \widetilde{w}}{\partial z} - \frac{4}{3}\,C_A\,\frac{\nu_t\,K}{\overline{\rho}\,\epsilon}\,\frac{\partial \overline{\rho}}{\partial z}\,\frac{\partial \overline{p}}{\partial z}\right),\end{aligned} \tag{184}$$

where the mean viscous stress tensor component is $\overline{\sigma}_{zz} = 2\overline{\mu}\,\partial\widetilde{w}/\partial z$ and the buoyancy-generalized Reynolds stress model is [20]

$$\tau_{zz} = \frac{2}{3}\,\overline{\rho}\,K - 2\,\mu_t\,\frac{\partial \widetilde{w}}{\partial z} - \frac{4}{3}\,C_A\,\frac{\nu_t\,K}{\overline{\rho}\,\epsilon}\,\frac{\partial \overline{\rho}}{\partial z}\,\frac{\partial \overline{p}}{\partial z} \tag{185}$$

with dimensionless coefficient C_A. Taking $C_A = 0$ reduces this to the standard Boussinesq Reynolds stress model. For Kelvin–Helmholtz mixing the mean shear velocity, $\widetilde{v}$, transport equation is

$$\begin{aligned}\overline{\rho}\left(\frac{\partial}{\partial t} + \widetilde{w}\,\frac{\partial}{\partial z}\right)\widetilde{v} &= \frac{\partial}{\partial z}\left(\overline{\mu}\,\frac{\partial \widetilde{v}}{\partial z} - \overline{\rho\,v''\,w''}\right) \\ &= \frac{\partial}{\partial z}\left[(\overline{\mu} + \mu_t)\,\frac{\partial \widetilde{v}}{\partial z}\right].\end{aligned} \tag{186}$$

These equations are closed with the previously constructed turbulent transport coefficients $\nu_t(z,t)$ and $D_t(z,t)$ obtained by solving the BSDS equations.

The approximate analytic solutions for the mean fields are given in Section 2.5 of Ref. [10], and are not repeated here.

8. Application of the general buoyancy–shear–drag–scalar turbulence model to Rayleigh–Taylor, reshocked Richtmyer–Meshkov, and Kelvin–Helmholtz mixing

Similar constant acceleration Rayleigh–Taylor, reshocked Richtmyer–Meshkov, and Kelvin–Helmholtz mixing cases considered previously in Ref. [10] are considered here. However, here the BSDS equations are solved numerically with $\Theta(t)$ an active scalar. The scalar will be assumed to be the heavy mass fraction for which $\overline{\phi} = 1/2$ is the average value in a mixed state and $At_\phi = 1$. For each instability, it will be assumed that $\theta_0 = 0.90$ at $t = 0$ and using Eqs. (53) and (59),

$$\Theta(0) = \Theta_0 = \sqrt{1-\theta_0}\,. \tag{187}$$

With a calibration to the values in Eq. (154) used in Ref. [10], the evolution of the mixing layer widths and of the mechanical turbulence fields is that shown in Ref. [10], and therefore are not reproduced here. The present model does not account for early-time entrainment that results in θ_m attaining a minimum value and then increasing to values ~ 0.8 at late times for all three instabilities in a self-similar state [7, 41, 42], as $\Theta(t)$ and $S(t)$ relax (slowly for the Rayleigh–Taylor case and very rapidly for the Richtmyer–Meshkov and Kelvin–Helmholtz cases) to their constant asymptotic values consistent with the chosen values of the molecular mixing parameter θ_{mol}. Only the evolution of the scalar and associated turbulent fields will be shown here.

The expressions (155)–(157) with $C^*_{vm} = 2$ will be used in the model applications below, where the full bubble and spike (rather than simplified bubble plus spike) equations will be solved numerically as in Ref. [10] using the *Mathematica*® function `NDSolve` (with the `StiffnessSwitching` Method option for the Richtmyer–Meshkov case). *Mathematica*® is also used to construct and evolve the scalar turbulent quantities

$$S(z,t) = S(t)\, f\left(\frac{z-z_{int}}{h_b(t)}, \frac{z-z_{int}}{h_s(t)}\right) \quad , \quad \chi(z,t) = C_\chi\, \frac{v(t)}{h(t)}\, S(z,t)\,, \tag{188}$$

$$\theta_m(z,t) = 1 - \frac{S(z,t)}{At_\phi^2\, \overline{\phi}^2} \tag{189}$$

in space and time. Note that $\theta_m(t) = \theta_m(0,t)$ is the 'centerline' value. To evolve the mean heavy mass fraction and mean shear velocity in Eqs. (63) and (72) in Ref. [10], the initial diffuse interface width $\delta_0 = 0.1$ cm is used (not shown here).

In the applications of the model below, the inverse parabolic–Gaussian profiles

$$f\left(\frac{z-z_{int}}{h_b(t)}, \frac{z-z_{int}}{h_s(t)}\right) = \left[1 + \frac{z-z_{int}}{h_b(t)}\right]\left[1 - \frac{z-z_{int}}{h_s(t)}\right] \exp\left[-\frac{(z-z_{int})^2}{h_b(t)\, h_s(t)}\right] \tag{190}$$

normalized to unity and restricted to positive values are used. Such profiles have tails at the edges of the mixing layer, qualitatively similar to those seen in experiments and numerical simulations. It is assumed that the light and heavy fluid occupy $z < z_{int}$ and $z > z_{int}$, where $z_{int} = 0$ is the interface location.

8.1. Application to Rayleigh–Taylor mixing

Consider the case of a constant acceleration ($\theta_{RT} = 2$), $g_0 = 981$ cm/s^2, $At = 0.5$, $\overline{\nu} = \overline{D} = 0.01$ cm^2/s, $h_{0,b} = h_{0,s} = 0.01$ cm, and $v_{0,b} = v_{0,s} = 0$. The final time is $t_f = 24$ s (longer than in Ref. [10] to better show the approach of the molecular mixing parameter to its calibrated late-time value).

Figure 1 shows the time-evolution of the normalized scalar fluctuation, scalar variance, and scalar variance dissipation rate, and Fig. 2 shows the corresponding evolution of the molecular mixing parameter $\theta_m(t)$. Both $\Theta(t)$ and $S(t)$ rapidly relax from their initial values and slowly approach their asymptotic values $\Theta(\infty) = \sqrt{1-\theta_{mol}} \approx 0.45$ and $S(\infty) = 0.05$. It is apparent that $\theta_m(t)$ relaxes very slowly to its asymptotic (calibrated) value 0.8.

Figures 3–5 show the spatiotemporal evolution of the scalar variance, scalar variance dissipation rate, and molecular mixing. The peak values of

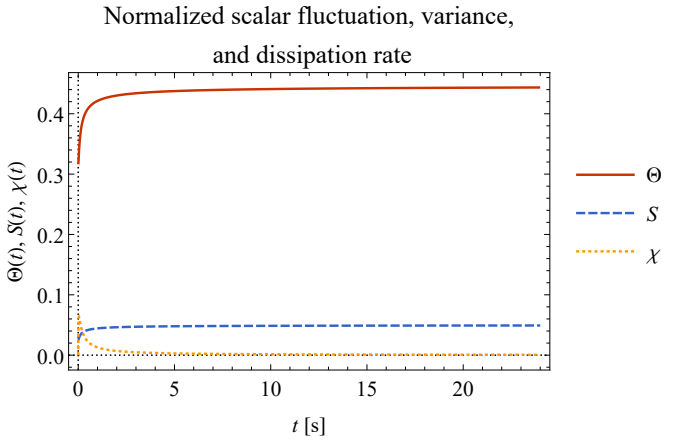

Figure 1: Time-evolution of the normalized scalar fluctuation, scalar variance, and scalar variance dissipation rate $\Theta(t)$, $S(t)$, and $\chi(t)$ for Rayleigh–Taylor mixing.

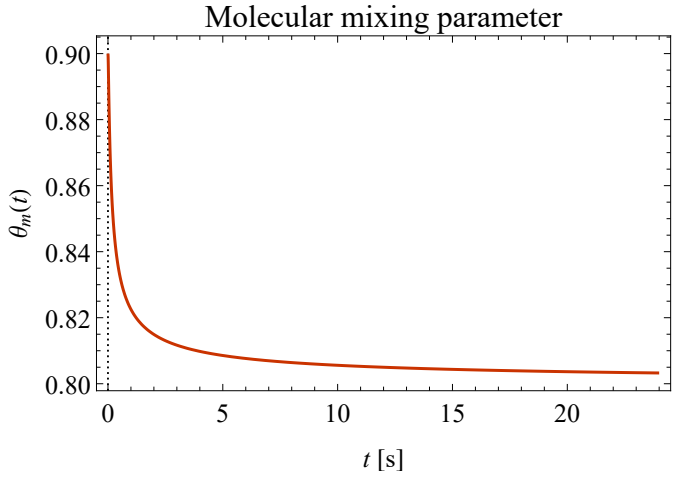

Figure 2: Time-evolution of the molecular mixing parameter $\theta_m(t)$ for Rayleigh–Taylor mixing.

the fields evolve with the expected late-time t^0, t^{-1}, and t^0 power-laws, respectively. The profiles are a maximum near the interface $z_{int} = 0$, exhibit increasing asymmetry toward the light (bubble) side as time evolves, and widen rapidly as the mixing layer width grows quadratically in time. The locations of the peak values also shift towards the bubble side at an increasing rate. The peak values of the profiles of S slowly approach 0.05 and the peak values of the profiles of $\theta_m(z,t)$ slowly approach 0.8, consistent with the approach of $\theta_m(t)$ to 0.8.

8.2. Application to reshocked Richtmyer–Meshkov mixing

With the same approximation used in Section 8.1 above, the mean equations for Rayleigh–Taylor mixing are formally the same for Richtmyer–Meshkov mixing. Let $\Delta v_s = 981$ cm/s^2, $\Delta v_r = 1.2\Delta v_s$ at $t_{res} = 5$ s, $At = 0.67$, $\overline{D} = 0.01$ cm^2/s, $\delta_0 = 0.1$ cm, $h_{0,b} = h_{0,s} = 0.01$ cm, and $v_{0,b} = v_{0,s} = \Delta v_s$. The acceleration representing the initial and second shock is taken as

$$g_{\text{eff}}(t) = \begin{cases} \frac{\Delta v_s}{10\, t_*} \exp\left(-10\, t^2/t_0^2\right) & \text{if } t < t_{res} \\ \frac{\Delta v_r}{10\, t_*} \exp\left[-10\,(t-t_{res})^2/t_0^2\right] & \text{if } t \geq t_{res} \end{cases}, \tag{191}$$

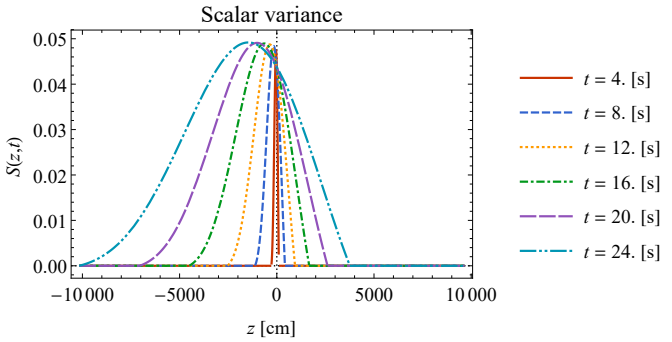

Figure 3: Spatiotemporal evolution of the scalar variance $S(z,t)$ for Rayleigh–Taylor mixing.

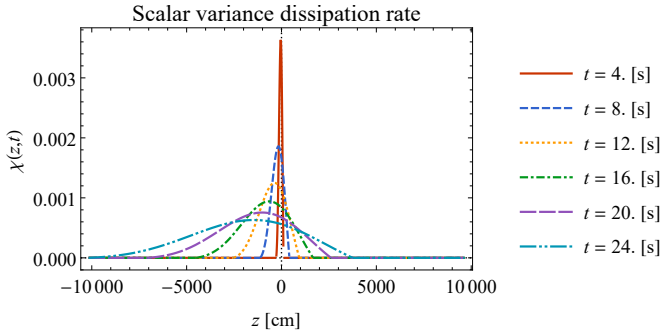

Figure 4: Spatiotemporal evolution of the scalar variance dissipation rate $\chi(z,t)$ for Rayleigh–Taylor mixing.

where $t_0 = 0.1$ s, the exponential factors make the acceleration zero for times between the first and second shocks, and are thus effectively delta functions at $t = 0$ and $t = t_{res}$. The final time is $t_f = 10$ s.

Figure 6 shows the time-evolution of the normalized scalar fluctuation, scalar variance, and scalar variance dissipation rate, and Fig. 7 shows the corresponding evolution of the molecular mixing parameter $\theta_m(t)$. Both $\Theta(t)$ and $S(t)$ rapidly attain their constant asymptotic values $\Theta(\infty) = \sqrt{1-\theta_{mol}} \approx 0.45$ and $S(\infty) = 0.05$, while $\chi(t)$ decays from its initial value, increases at the time of reshock, and then continues to decay. It is also apparent that $\theta_m(t)$ also attains its asymptotic (calibrated) value 0.8 almost immediately; a very slight change can be seen at the time of reshock.

Figures 8–10 show the spatiotemporal evolution of the scalar variance, scalar variance dissipation rate, and molecular mixing. Again, the peak values of the fields evolve with the expected late-time t^0, t^{-1}, and t^0 power-laws, respectively. At early times, the profiles are a maximum near the interface $z_{int} = 0$ and exhibit increasing asymmetry toward the light (bubble) side as time evolves, and particularly after reshock when the profiles widen more rapidly as the mixing layer width grows more rapidly after reshock than before reshock. The scalar variance dissipation rate rapidly decreases in magnitude, is increased at the time or reshock, and then decays rapidly. The peak values of the molecular mixing parameter profiles are 0.8.

8.3. Application to Kelvin–Helmholtz mixing

Let $g(t) = 0$, $v_b = 900$ cm/s, $v_s = 1500$ cm/s, $\Delta v = 600$ cm/s, $At = 0$, $\overline{\nu} = 0.01$ cm^2/s, $\delta_0 = 0.1$ cm, $h_{0,b} = h_{0,s} = 0.01$ cm, and $v_{0,b} = v_{0,s} = 0$. Also, $At_v = |(v_s - v_b)/(v_s + v_b)| = 0.25$. In this case, the mixing layer parameter δ does not depend on θ_{mol} because both streams have the same density (the scalar is passive). However, each stream could be assigned a scalar tracer. The final time is $t_f = 10$ s.

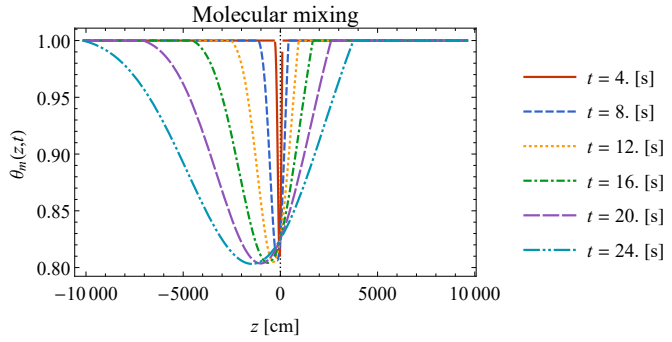

Figure 5: Spatiotemporal evolution of the molecular mixing $\theta_m(z,t)$ for Rayleigh–Taylor mixing.

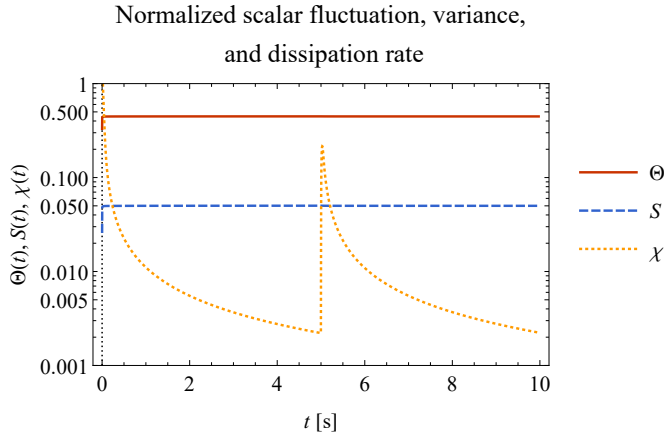

Figure 6: Time-evolution of the normalized scalar fluctuation, scalar variance, and scalar variance dissipation rate $\Theta(t)$, $S(t)$, and $\chi(t)$ for reshocked Richtmyer–Meshkov mixing.

Figure 11 shows the time-evolution of the normalized scalar fluctuation, scalar variance, and scalar variance dissipation rate, and Fig. 12 shows the corresponding evolution of the molecular mixing parameter $\theta_m(t)$. Both $\Theta(t)$ and $S(t)$ almost immediately attain their constant asymptotic values $\Theta(\infty) = \sqrt{1-\theta_{mol}} \approx 0.45$ and $S(\infty) = 0.05$. The scalar variance dissipation rate $\chi(t)$ decays from its initial value. It is also apparent that $\theta_m(t)$ almost immediately attains its asymptotic (calibrated) value 0.8.

Figures 13–15 show the spatiotemporal evolution of the scalar variance, scalar variance dissipation rate, and molecular mixing. Again, the peak values of the fields evolve with the expected late-time t^0, t^{-1}, and t^0 power-laws, respectively. The profiles are a maximum near the interface $z_{int} = 0$ and widen as the mixing layer width grows linearly in time. The profiles remain symmetric about the interface because $At = 0$.

9. Summary, discussion, and conclusions

The theoretical buoyancy–shear–drag–scalar-based turbulence model developed and demonstrated here for binary power-law acceleration driven Rayleigh–Taylor, reshocked Richtmyer–Meshkov, and Kelvin–Helmholtz mixing is based on the observation that the evolution of the mean fields is fundamentally determined by a turbulent diffusivity and viscosity (as assumed in the original mixing-length turbulence models) if gradient-diffusion models are used to close the turbulent fluxes in the mean transport equations, i.e., equations for the turbulent kinetic energy and another quantity (turbulent kinetic energy dissipation rate or lengthscale) are not

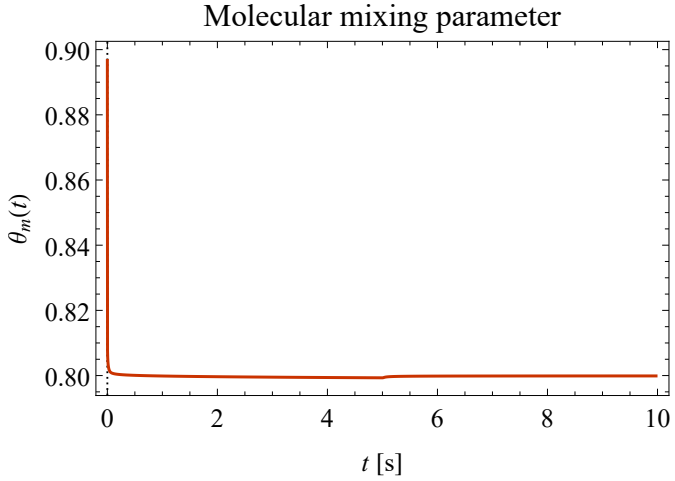

Figure 7: Time-evolution of the molecular mixing parameter $\theta_m(t)$ for reshocked Richtmyer–Meshkov mixing.

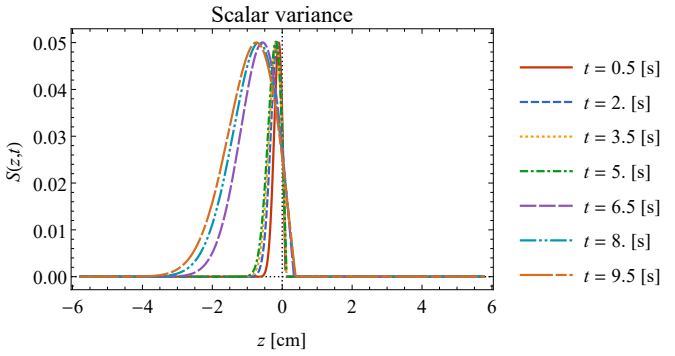

Figure 8: Spatiotemporal evolution of the scalar variance $S(z,t)$ for reshocked Richtmyer–Meshkov mixing.

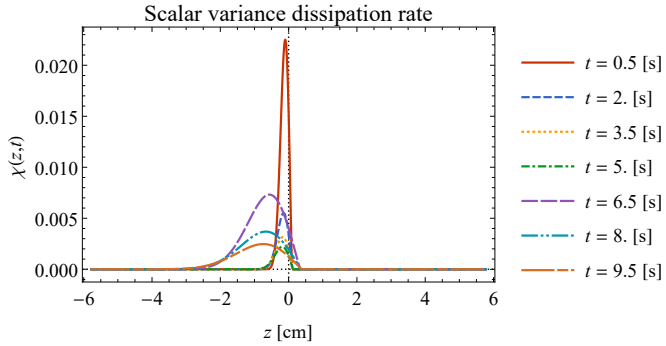

Figure 9: Spatiotemporal evolution of the scalar variance dissipation rate $\chi(z,t)$ for reshocked Richtmyer–Meshkov mixing.

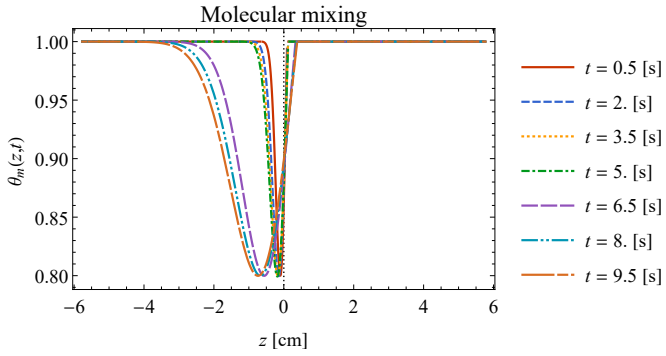

Figure 10: Spatiotemporal evolution of the molecular mixing $\theta_m(z,t)$ for reshocked Richtmyer–Meshkov mixing.

essential because the turbulent transport coefficients can be constructed directly from the mixing layer width and mixing layer velocity (and assumed spatiotemporal profiles).

In summary, the modeling framework proposed here can be used in three ways:

1. as a pure buoyancy–shear–drag–scalar (BSDS) model for time-dependent mixing layer widths and scalars, and any quantities constructed from them;
2. using the BSDS solutions to construct a turbulent diffusivity and viscosity with assumed spatially and temporally evolving spatial profiles similar to self-similar profiles, and numerically evolving approximate self-similar mean fields;
3. using the BSDS solutions to construct a turbulent diffusivity and viscosity with assumed spatially and temporally evolving spatial profiles similar to self-similar profiles, and solving the closed mean field equations numerically.

The present model equations combine the previously developed buoyancy–shear–drag model [10] with a scalar variance equation and an algebraic model for the scalar variance dissipation rate, allowing the model to describe active or passive scalar mixing. An equation for the scalar variance dissipation rate was also derived and could be solved instead of using an algebraic model (however, this would require calibrating additional model coefficients). This quasi-homogeneous model can be regarded as intermediate between an ordinary differential BSDS model and a partial differential Reynolds-averaged transport model. Although the model is presently formulated for planar geometries, it is still true that the most detailed experimental and simulation data concerning interfacial instability-induced mixing also corresponds to planar geometry. Spatial, temporal, and diagnostic limitations of experiments and simulations in convergent or divergent geometries currently preclude detailed measurements in such geometries. Reference [10] provides additional background on the overall motivation and theoretical approach to constructing a turbulence model from such equations.

First, beginning with a general equation for a fluctuating scalar ϕ', the corresponding equation for the scalar variance $S = \overline{\phi'^2}$ was constructed. This equation was closed using gradient-diffusion concepts and an algebraic closure for the scalar variance dissipation rate χ. Alternatively, a closed equation for χ was derived phenomenologically from the S equation using a scale-similarity assumption similar to that used in Reynolds-averaged modeling of the turbulent scalar variance dissipation rate equation. The scalar variance equation requires two coefficients C_p and C_χ if an algebraic model is used for χ. Using a differential model equation for χ in general adds three coefficients (and removes one coefficient, C_χ, from the S equation), requiring additional physical quantities for their calibration.

Nonlinear analytical self-similar solutions were derived for the scalar variance as a function of the mixing layer width $h(t)$ and the model coefficients. The calibration of the scalar variance production coefficient using a value of the asymptotic molecular mixing parameter θ_{mol} was described. Early- and late-time solutions of the BSDS equations were derived analytically for both miscible and immiscible mixing and each instability. As expected, the early-time solutions depend on the initial conditions, while the late-time solutions are independent of the initial conditions. The temporal power-law exponents of the early-time mixing layer widths depend on the scalar variance dissipation rate coefficient, while the exponents of the late-time widths do not. For the power-law-in-time acceleration-driven

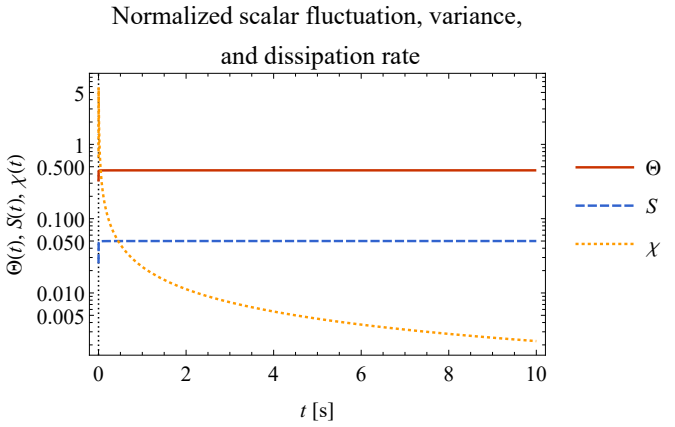

Figure 11: Time-evolution of the normalized scalar fluctuation, scalar variance, and scalar variance dissipation rate $\Theta(t)$, $S(t)$, and $\chi(t)$ for Kelvin–Helmholtz mixing.

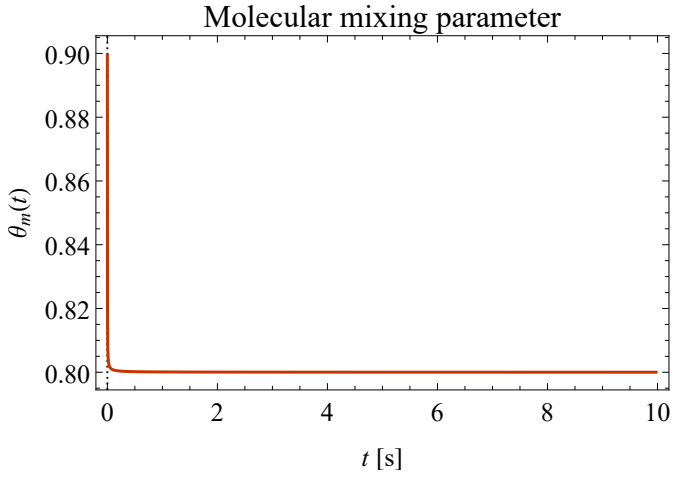

Figure 12: Time-evolution of the molecular mixing parameter $\theta_m(t)$ for Kelvin–Helmholtz mixing.

Rayleigh–Taylor case and the Kelvin–Helmholtz instability case, expressions for the mixing layer growth parameters α and δ that depend on the degree of molecular mixing through the factors $\sqrt{1-\theta_{mol,RT}}$ and $1-\theta_{mol,KH}$, respectively, and expressions for the scalar variance were derived. A time-dependent expression for α was also derived in the fully-atomic mixing case. While the Richtmyer–Meshkov mixing layer width does not depend on the degree of molecular mixing, an expression for the passive scalar variance was derived. For each instability, solutions were derived for the miscible mixing case with $\theta_{mol} \in (0,1)$ corresponding to a scalar variance production coefficient $0 < C_p < C_\chi$, as well as for the fully-atomic miscible mixing case with $\theta_{mol} = 1$ and $C_p = 0$ and for the immiscible mixing case with $\theta_{mol} = 0$ and $C_p = C_\chi$. Analytical solutions corresponding to decaying scalar instability-induced turbulence were used to calibrate the scalar variance dissipation coefficient C_χ for each instability: in this formulation, the relationship between $h(t)$ and $v(t)$, $v/h = \theta_h/t$, introduces a dependence of C_χ on the instability exponent θ_h. A universal calibration of C_χ based on decaying isotropic scalar turbulence was also presented. The calibration method is analogous to that used in the self-similar approximation of Reynolds-averaged turbulence models [7]. The corresponding analytical solutions and calibrations were also derived for the general model with separate bubble and spike equations coupled to the scalar variance equation.

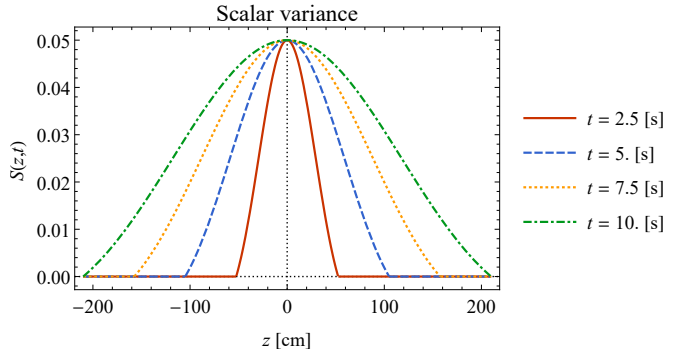

Figure 13: Spatiotemporal evolution of the scalar variance $S(z,t)$ for Kelvin–Helmholtz mixing.

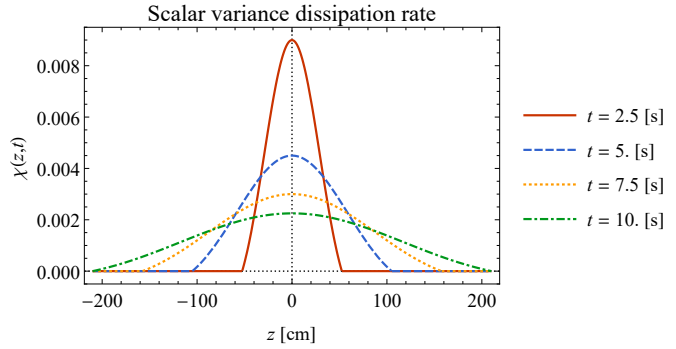

Figure 14: Spatiotemporal evolution of the scalar variance dissipation rate $\chi(z,t)$ for Kelvin–Helmholtz mixing.

The BSDS equations for the bubble and spike were then solved numerically for constant acceleration Rayleigh–Taylor, reshocked Richtmyer–Meshkov, and Kelvin–Helmholtz mixing using model coefficients calibrated to specific values of the mixing layer growth parameters and exponents $\alpha = 0.05$, $\theta = 0.30$, and $\delta = 0.07$ and to the typical value $\theta_{mol} = 0.8$. The time-evolutions of $S(t)$, $\chi(t)$, and $\theta_m(t)$ were shown to be consistent with the calibration of the model to $\theta_{mol} = 0.8$ for each instability case. The corresponding spatial profiles were constructed using the procedure described in Ref. [10] and assumed self-similar inverse parabolic–Gaussian spatial profiles depending on the mixing layer widths $h_b(t)$ and $h_s(t)$. The spatiotemporal evolution of the fields $S(z,t)$, $\chi(z,t)$, and $\theta_m(z,t)$ were shown to be consistent with expectations, including bubble and spike side asymmetries in the spatial profiles of the fields for the Rayleigh–Taylor and Richtmyer–Meshkov cases having $At \neq 0$. The mechanical fields are those shown in Ref. [10], and were not reconstructed here, while the scalar variance and its dissipation rate evolved qualitatively similarly to the self-similar fields in Ref. [7] (where inverse parabolic profiles were used to obtain the analytic solutions for the fields).

The theoretical zero-dimensional (i.e., ordinary differential) or one-dimensional (i.e., with phenomenologically constructed or numerically computed mean and turbulent fields) model developed conceptually by utilizing the temporal and spatial separability of self-similar turbulent fields and demonstrated here serves several pedagogical and practical purposes. Analytical and numerical solutions of the model can be used to build a fundamental understanding of the instability and mixing dynamics arising from classical interfacial instabilities as well as from combined instabilities. The exact and approximate analytical solutions of the nonlinear ordinary differential equations exhibit the dependence of the solutions on the physical parameters and model coefficients. Exploiting parallels with Reynolds-averaged turbulence models, the coefficients in the present model can be systematically calibrated using physical observables. The

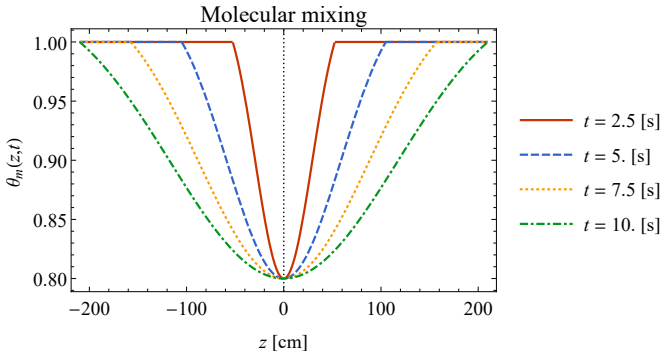

Figure 15: Spatiotemporal evolution of the molecular mixing $\theta_m(z,t)$ for Kelvin–Helmholtz mixing.

model can be used to rapidly estimate mixing layer widths, molecular mixing parameters, turbulent fields, and many other quantities derived from these.

The model can also be applied to very large Reynolds number astrophysical, inertial confinement fusion, and high-energy-density physics flows where turbulence and mixing have an important role and remain challenging to model physically and numerically. For example, the present model would be much better than a simple fall-line mixing model [43] still extensively used in ICF modeling. As the temporal scalings of the self-similar solutions of the BSDS model equations for each instability are the same as those in the K–ϵ–S–χ model [7] (but with coefficients specific to the present model), the model could serve as a much simpler alternative to the full Reynolds-averaged turbulence model. The model can be used to develop and evaluate new concepts before implementation in a full turbulence model. As discussed in Ref. [10], the model can be applied to flows with time-varying densities, general time-dependent accelerations, include de(compression) and compressibility effects, include molecular viscosity and diffusivity effects, ablation, and consider early-time linear instability evolution.

Further refinements of this model are possible, including investigating alternative closures of the terms in the equations, developing model modifications that describe transition to turbulence (such as an intermittency model [44]), using the scalar variance dissipation rate equation rather than an algebraic model to potentially improve molecular mixing modeling, developing hybridized model coefficients to better describe combined instabilities, refining the assumed spatial profiles, and formulating the equations in radial geometry. Modifications to the model that can describe the transitional evolution of $h(t)$ and $\theta_m(t)$ for example in Rayleigh–Taylor mixing would provide improved early-time predictions of experimental and simulation data [45]. The model can also be used in analogy with traditional buoyancy–drag models without solving for (or constructing) turbulent fields. Future comparisons of the predictions of this model to experimental and numerical simulation data will evaluate the predictive capabilities and limitations of the model, and also suggest other potential improvements.

Acknowledgements

This research was originally presented at the 17th International Workshop on the Physics of Compressible Turbulent Mixing (IWPCTM) in Atlanta, Georgia (July 2022). This work was performed under the auspices of the U.S. Department of Energy by Lawrence Livermore National Laboratory under Contract No. DE-AC52-07NA27344.

References

[1] Y. Zhou, R. J. R. Williams, P. Ramaprabhu, M. Groom, B. Thornber, A. Hillier, W. A. Mostert, B. Rollin, S. Balachandar, P. D. Powell, A. Mahalov, N. Attal, Rayleigh–Taylor and Richtmyer–Meshkov instabilities: A journey through scales, Physica D 423 (2021) 132838–1–132838–86.

[2] C. Eckart, An analysis of the stirring and mixing processes in incompressible fluids, Journal of Marine Research 7 (1948) 265–275.

[3] D. Besnard, F. H. Harlow, R. M. Rauenzahn, C. Zemach, Turbulence transport equations for variable-density turbulence and their relationship to two-field models, Tech. Rep. LA-12303-MS, Los Alamos National Laboratory, Los Alamos, New Mexico (1992).

[4] O. Grégoire, D. Souffland, S. Gauthier, A second-order turbulence model for gaseous mixtures induced by Richtmyer–Meshkov instability, Journal of Turbulence 6 (2005) 29–1–29–20.

[5] B. E. Morgan, B. J. Olson, W. J. Black, J. McFarland, Large-eddy simulation and Reynolds-averaged Navier-Stokes modeling of a reacting Rayleigh-Taylor mixing layer in a spherical geometry, Physical Review E 98 (2018) 033111–1–033111–21.

[6] J. R. Ristorcelli, Exact statistical results for binary mixing and reaction in variable density turbulence, Physics of Fluids 29 (2017) 020705–1–020705–12.

[7] O. Schilling, Self-similar Reynolds-averaged mechanical–scalar turbulence models for Rayleigh–Taylor, Richtmyer–Meshkov, and Kelvin–Helmholtz instability-induced mixing in the small Atwood number limit, Physics of Fluids 33 (2021) 085129–1–085129–43.

[8] O. Schilling, Self-similar Reynolds-averaged mechanical–scalar turbulence models for reshocked Richtmyer–Meshkov instability-induced mixing in the small Atwood number limit, Physics of Fluids 36 (2024) 015149–1–015149–13.

[9] O. Schilling, Self-similar Reynolds-averaged mechanical–scalar turbulence models for Rayleigh–Taylor mixing induced by power-law accelerations in the small Atwood number limit, Physics of Fluids 36 (2024) 075170–1–075170–17.

[10] O. Schilling, A buoyancy–shear–drag-based turbulence model for Rayleigh–Taylor, reshocked Richtmyer–Meshkov, and Kelvin–Helmholtz mixing, Physica D 402 (2020) 132238–1–132238–14.

[11] D. L. Youngs, B. Thornber, Early time modifications to the buoyancy-drag model for Richtmyer–Meshkov mixing, ASME Journal of Fluid Engineering 142 (2020) 121107–1–121107–7.

[12] B. Thornber, J. Griffond, O. Poujade, N. Attal, H. Varshochi, P. Bigdelou, P. Ramaprabhu, B. Olson, J. Greenough, Y. Zhou, O. Schilling, K. A. Garside, R. J. R. Williams, C. A. Batha, P. A. Kuchugov, M. E. Ladonkina, V. F. Tishkin, N. V. Zmitrenko, V. B. Rozanov, D. L. Youngs, Late-time growth rate, mixing, and anisotropy in the multimode narrowband Richtmyer–Meshkov instability: The θ-group collaboration, Physics of Fluids 29 (2017) 105107–1–105107–24.

[13] D. L. Youngs, B. Thornber, Buoyancy–Drag modelling of bubble and spike distances for single-shock Richtmyer–Meshkov mixing, Physica D 410 (2020) 132517–1–132517–19.

[14] M. E. Rafei, B. Thornber, Numerical study and buoyancy–drag modeling of bubble and spike distances in three-dimensional spherical implosions, Physics of Fluids 32 (2020) 124107–1–124107–19.

[15] A. Llor, Bulk turbulent transport and structure in Rayleigh-Taylor, Richtmyer-Meshkov, and variable acceleration instabilities, Laser and Particle Beams 21 (2003) 305–310.

[16] A. Llor, Statistical Hydrodynamic Models for Developed Mixing Instability Flows: Analytical "0D" Evaluation Criteria, and Comparison to Single- and Two-Phase Flow Approaches, Lecture Notes in Physics Vol. 681, Springer-Verlag, New York, NY, 2005.

[17] D. Shvarts, U. Alon, D. Ofer, R. L. McCrory, C. P. Verdon, Nonlinear evolution of multimode Rayleigh-Taylor instability in two and three dimensions, Physics of Plasmas 2 (1995) 2465–2472.

[18] S. I. Abarzhi, Interlinking Rayleigh–Taylor/Richtmyer–Meshkov interfacial mixing with variable acceleration and canonical Kolmogorov turbulence, Physics of Fluids 36 (2024) 072102–1–072102–22.

[19] S. I. Abarzhi, D. L. Hill, K. C. Williams, J. T. Li, B. A. Remington, D. Martinez, W. D. Arnett, Fluid dynamic mathematical aspects of supernova remnants, Physics of Fluids 35 (2023) 034106–1–034106–22.

[20] O. Schilling, N. J. Mueschke, Analysis of turbulent transport and mixing in transitional Rayleigh–Taylor unstable flow using direct numerical simulation data, Physics of Fluids 22 (2010) 105102–1–105102–26.

[21] O. Schilling, N. J. Mueschke, Turbulent transport and mixing in transitional Rayleigh-Taylor unstable flow: *A priori* assessment of gradient-diffusion and similarity modeling, Physical Review E 96 (2017) 063111–1–063111–26.

[22] S. I. Abarzhi, A. Gorobets, K. R. Sreenivasan, Rayleigh-Taylor turbulent mixing of immiscible, miscible and stratified fluids, Physics of Fluids 17 (2005) 081705–1–081705–4.

[23] L. D. Landau, E. M. Lifshitz, Fluid Mechanics, 2nd Edition, Course of Theoretical Physics Vol. 6, Pergamon Press, New York, NY, 1987.

[24] G. Boffetta, A. Mazzino, S. Musacchio, L. Vozella, Statistics of mixing in three-dimensional Rayleigh–Taylor turbulence at low Atwood number and Prandtl number one, Physics of Fluids 22 (2010) 035109–1–035109–8.

[25] G. Boffetta, A. Mazzino, Incompressible Rayleigh–Taylor turbulence, Annual Review of Fluid Mechanics 49 (2017) 119–143.

[26] N. J. Mueschke, M. J. Andrews, O. Schilling, Experimental characterization of initial conditions and spatio-temporal evolution of a small-Atwood-number Rayleigh–Taylor mixing layer, Journal of Fluid Mechanics 567 (2006) 27–63.

[27] N. J. Mueschke, O. Schilling, Investigation of Rayleigh–Taylor turbulence and mixing using direct numerical simulation with experimentally measured initial conditions. I. Comparison to experimental data, Physics of Fluids 21 (2009) 014106–1–014106–19.

[28] N. J. Mueschke, O. Schilling, D. L. Youngs, M. J. Andrews, Measurements of molecular mixing in a high Schmidt number Rayleigh–Taylor mixing layer, Journal of Fluid Mechanics 632 (2009) 17–48.

[29] D. T. Reese, A. M. Ames, C. D. Noble, J. G. Oakley, D. A. Rothamer, R. Bonazza, Simultaneous direct measurements of concentration and velocity in the Richtmyer–Meshkov instability, Journal of Fluid Mechanics 849 (2018) 541–575.

[30] B. E. Morgan, Scalar mixing in a Kelvin-Helmholtz shear layer and implications for Reynolds-averaged Navier-Stokes modeling of mixing layers, Physical Review E 103 (2021) 053108–1–053108–15.

[31] P. Ramaprabhu, M. J. Andrews, Experimental investigation of Rayleigh–Taylor mixing at small Atwood numbers, Journal of Fluid Mechanics 502 (2004) 233–271.

[32] B. Gréa, The rapid acceleration model and the growth rate of a turbulent mixing zone induced by Rayleigh-Taylor instability, Physics of Fluids 25 (2013) 015118–1–015118–20.

[33] D. L. Youngs, The density ratio dependence of self-similar Rayleigh–Taylor mixing, Philosophical Transactions of the Royal Society of London A 371 (2013) 20120173–1–20120173–15.

[34] O. Schilling, Reynolds-averaged Navier–Stokes modeling of turbulent Rayleigh–Taylor, Richtmyer–Meshkov, and Kelvin–Helmholtz mixing using a higher-order shock-capturing method, in: Proceedings of the ASME - JSME - KSME Joint Fluids Engineering Conference 2019, American Society of Mechanical Engineers, 2019, pp. AJKFLUIDS2019–5235.

[35] J. T. Móran-López, O. Schilling, Multicomponent Reynolds-averaged Navier–Stokes simulations of reshocked Richtmyer–Meshkov instability-induced mixing, High Energy Density Physics 9 (2013) 112–121.

[36] J. T. Móran-López, O. Schilling, Multi-component Reynolds-averaged Navier–Stokes simulations of Richtmyer–Meshkov instability and mixing induced by reshock at different times, Shock Waves 24 (2014) 325–343.

[37] M. M. Rogers, R. D. Moser, Direct simulation of a self-similar turbulent mixing layer, Physics of Fluids 6 (2018) 903–923.

[38] S. B. Pope, Turbulent Flows, Cambridge University Press, 2000.

[39] B. E. Morgan, Self-consistent, high-order spatial profiles in a model for two-fluid turbulent mixing, Physical Review E 104 (2021) 015107–1–015107–14.

[40] Y.-s. Zhang, Z.-w. He, H.-s. Xie, M.-J. Xiao, B.-l. Tian, Methodology for determining coefficients of turbulent mixing model, Journal of Fluid Mechanics 905 (2020) A26–1–A26–40.

[41] Y. Zhou, Rayleigh–Taylor and Richtmyer–Meshkov instability induced flow, turbulence, and mixing. I, Physics Reports 720–722 (2017) 1–136.

[42] Y. Zhou, Rayleigh–Taylor and Richtmyer–Meshkov instability induced flow, turbulence, and mixing. II, Physics Reports 723–725 (2017) 1–160.

[43] S. V. Weber, D. T. Casey, D. C. Eder, J. D. Kilkenny, J. E. Pino, V. A. Smalyuk, G. P. Grim, B. A. Remington, D. P. Rowley, C. B. Yeamans, R. E. Tipton, M. Barrios, R. Benedetti, L. Berzak Hopkins, D. L. Bleuel, E. J. Bond, D. K. Bradley, J. A. Caggiano, D. A. Callahan, C. J. Cerjan, D. S. Clark, L. Divol, D. H. Edgell, M. J. Edwards, M. J. Eckart, D. Fittinghoff, J. A. Frenje, M. Gatu-Johnson, V. Y. Glebov, S. Glenn, N. Guler, S. W. Haan, A. Hamza, R. Hatarik, M. Herrmann, D. Hoover, W. W. Hsing, N. Izumi, O. S. Jones, M. Kervin, S. Khan, J. Kline, J. Knauer, A. Kritcher, G. Kyrala, O. L. Landen, S. Le Pape, T. Ma, A. J. Mackinnon, A. G. MacPhee, M. M. Marinak, J. M. Mcnaney, N. B. Meezan, F. E. Merrill, M. Mintz, A. Moore, D. H. Munro, A. Nikroo, A. Pak, T. Parham, R. Petrasso, H. G. Rinderknecht, D. B. Sayre, S. M. Sepke, B. K. Spears, W. Stoeffl, R. Tommasini, R. P. Town, P. Volegov, K. Widmann, D. C. Wilson, A. B. Zylstra, Simulations of indirectly driven gas-filled capsules at the National Ignition Facility, Physics of Plasmas 21 (2014) 112706–1–112706–9.

[44] H. Xie, H. Qi, M. Xiao, Y. Zhang, Y. Zhao, An intermittency based Reynolds-averaged transition model for mixing flows induced by interfacial instabilities, Journal of Fluid Mechanics 1002 (2025) A31–1–A31–28.

[45] O. Schilling, Progress on understanding Rayleigh–Taylor flow and mixing using synergy between simulation, modeling, and experiment, ASME Journal of Fluids Engineering 142 (2020) 120802–1–120802–25.